PLOS GENETICS

RESEARCH ARTICLE

HES1 is a novel downstream modifier of the SHH-GLI3 Axis in the development of preaxial polydactyly

Deepika Sharma[1,2], Anthony J. Mirando[1], Abigail Leinroth[1,3], Jason T. Long[1,3], Courtney M. Karner[1,3], Matthew J. Hilton[1,3]*

1 Department of Orthopedic Surgery, Duke University School of Medicine, Durham, North Carolina, United States of America, **2** Department of Biomedical Genetics, University of Rochester School of Medicine, Rochester, New York, United States of America, **3** Department of Cell Biology, Duke University, Durham, North Carolina, United States of America

* matthew.hilton@duke.edu

Citation: Sharma D, Mirando AJ, Leinroth A, Long JT, Karner CM, Hilton MJ (2021) HES1 is a novel downstream modifier of the SHH-GLI3 Axis in the development of preaxial polydactyly. PLoS Genet 17(12): e1009982. https://doi.org/10.1371/journal.pgen.1009982

Editor: FANXIN LONG, Children's Hospital of Philadelphia, UNITED STATES

Received: September 30, 2020

Accepted: December 7, 2021

Published: December 20, 2021

Data Availability Statement: All relevant data are within the manuscript and its Supporting Information files to be supplied.

Funding: This work was supported in part by the following United States National Institute of Health grants: R01 grants AR057022, AR063071, and AR071722 to MJH. The funders had no role in study design, data collection and analysis, decision to publish, or preparation of the manuscript.

Competing interests: The authors have declared that no competing interests exist.

Abstract

Sonic Hedgehog/GLI3 signaling is critical in regulating digit number, such that Gli3-deficiency results in polydactyly and Shh-deficiency leads to digit number reductions. SHH/GLI3 signaling regulates cell cycle factors controlling mesenchymal cell proliferation, while simultaneously regulating *Grem1* to coordinate BMP-induced chondrogenesis. SHH/GLI3 signaling also coordinates the expression of additional genes, however their importance in digit formation remain unknown. Utilizing genetic and molecular approaches, we identified HES1 as a downstream modifier of the SHH/GLI signaling axis capable of inducing preaxial polydactyly (PPD), required for Gli3-deficient PPD, and capable of overcoming digit number constraints of Shh-deficiency. Our data indicate that HES1, a direct SHH/GLI signaling target, induces mesenchymal cell proliferation via suppression of *Cdkn1b*, while inhibiting chondrogenic genes and the anterior autopod boundary regulator, *Pax9*. These findings establish HES1 as a critical downstream effector of SHH/GLI3 signaling in the development of PPD.

Author summary

Sonic Hedgehog/GLI3 signaling is critical in regulating digit number, such that Gli3-deficiency results in additional digits and Shh-deficiency leads to digit number reductions. SHH/GLI3 signaling within the developing limb regulates numerous genes critical for proper autopod (hand/foot) development, however not all target genes are known to be truly important for digit formation. Utilizing genetic and molecular approaches, we identified HES1 as a downstream modifier of the SHH/GLI signaling axis capable of inducing preaxial polydactyly (PPD), required for Gli3-deficient PPD, and capable of overcoming digit number constraints of Shh-deficiency. We further propose a mechanistic model by which HES1 coordinates the expression of genes important for proper digit development. These findings establish HES1 as a critical downstream effector of SHH/GLI3 signaling in the development of PPD.

Introduction

Development of the vertebrate limb is dependent on two signaling centers, the apical ectodermal ridge (AER) that controls proximal-distal (P-D) outgrowth and the zone of polarizing activity (ZPA), the source of *Sonic hedgehog* (*Shh*), which regulates anterior-posterior (A-P) patterning, digit number, and identity[1–4]. Prior to ZPA establishment within the distal posterior mesenchyme, an early A-P axis is first initiated via the expression of *Gli family zinc finger 3* (*Gli3*) and *Aristaless-like 4* (*Alx4*) within the anterior limb bud mesenchyme. GLI3 restricts the expression of *Heart and neural crest derivatives-expressed protein 2* (*Hand2*) to the posterior mesenchyme, while HAND2 antagonizes *Gli3* and *Alx4* expression[5]. This antagonistic relationship pre-patterns the mesenchyme allowing for the initiation of *Shh* within the posterior mesenchyme via the action of Fibroblast Growth Factors (FGFs) secreted from the AER [6,7]. SHH in turn enforces *Fgf* expression (primarily *Fgf8* and *Fgf4*) within the AER, establishing a positive feedback loop that maintains both signaling centers and keeps cells within the distal mesenchyme or apical zone (AZ) in a proliferative and undifferentiated state prior to chondrogenic differentiation and digit formation[8,9].

During A-P patterning of the limb bud, SHH signals in a posterior to anterior manner from the ZPA to inhibit GLI3 protein processing from the full-length activator (GLI3A) to the truncated repressor (GLI3R), thereby restricting the highest concentrations of GLI3R to the anterior limb bud mesenchyme[10]. SHH-mediated regulation of GLI3 processing is critical for establishing the pentadactylous autopod with proper digit identities. Germline mutations of *Gli3* lead to multiple forms of polydactyly, and in humans is the underlying cause for Greig cephalopolysyndactyly syndrome (OMIM: 175700), Pallister-Hall syndrome (OMIM: 146510), postaxial polydactyly types A1 and B (OMIM: 174200), and preaxial polydactyly type IV (OMIM: 174700). Conventional homozygous gene deletion of *Gli3* in the mouse, represented by the *extra-toes* mutation ($Gli3^{xt/xt}$), results in the development of generalized polydactyly (seven or greater digits without obvious identities), while heterozygous deletion or haploinsufficiency leads to the development of a single anterior extra digit or preaxial polydactyly (PPD) [11,12]. Conversely, germline homozygous deletion of *Shh* results in the development of only a single anterior digit with digit one identity due to the preponderance of GLI3R throughout the limb bud mesenchyme, directly implicating the SHH-GLI3 signaling axis in regulating digit number and identity[5,13,14]. Therefore, a primary function of SHH within the autopod is to counteract the GLI3R-mediated constraints on digit development, and this dominance of GLI3R-mediated regulation of digit number and identity is highlighted by the indistinguishable forms of polydactyly observed in $Gli3^{xt/xt}$ mutant and $Shh^{-/-}$; $Gli3^{xt/xt}$ compound mutant mice[15,16].

Mechanistically, the SHH-GLI3 signaling axis regulates the expression of numerous factors implicated in coordinating digit number and/or identity during limb development. Unbiased gene expression studies have identified a few hundred potential candidates likely to be regulated directly or indirectly by SHH and GLI transcription factors[17,18]. However, many of these genes, such as *Hoxd10-13*[19–21], *Hand2*[22], *Alx4*[23], *Twist1*[24,25], *Fgf4*[26], *Fgf8* [26,27], *Etv4*[25,28], *Etv5*[25,28], *Tbx2*[29,30], *Tbx3*[30], *Gata6*[31], and others, also in turn directly regulate *Shh/Gli3* expression and signaling that results in a feedback loop impacting digit development. Recent genetic interaction and functional studies determined that one model by which GLI3R functions to constrain digit number requires the coordinated suppression of downstream cell cycle regulators, *Cyclin d1* (*Ccnd1*) and *Cyclin dependent kinases 2*, *4*, *and 6* (*Cdk2*, *Cdk4*, *Cdk6*), and the Bone Morphogenetic Protein (BMP) antagonist, *Gremlin (Grem1)*(32). To control size of the limb field and digit number, this gene regulation ensures that SHH-GLI3 signaling simultaneously coordinates mesenchymal progenitor cell

proliferation and the timing by which BMP signaling induces digit chondrogenesis[32]. Additional factors have been identified that potentially function downstream of the SHH-GLI3 signaling without known feedback regulation, these factors include *Paired box 9* (*Pax9*) and several NOTCH signaling pathway components, *Jagged1* (*Jag1*), *Hairy/enhancer-of-split 1* (*Hes1*), *and Hairy/enhancer-of-split related with YRPW motif protein 1* (*Hey1*)[17,18,33]. *Pax9* is expressed in the anterior mesenchyme of the limb bud and when deleted gives rise to a single anterior extra digit without obvious alterations to *Shh/Gli3* expression or signaling[34]. In a reciprocal fashion, *Jag1*, *Hey1*, *and Hes1* are expressed in the posterior distal mesenchyme of the limb bud overlapping the ZPA (*Shh* expression) and surrounding mesenchyme[33,35–37]. Genetic evidence and gene expression studies suggest that each of these genes may be regulated by SHH-GLI3 signaling, such that deletion of *Gli3* results in an anterior expansion of *Jag1*, *Hey1*, and *Hes1* expression with the concomitant loss of *Pax9* within the anterior mesenchyme of the limb bud[33,36]. Further, cis-regulatory analyses identified GLI-consensus DNA binding sites and SHH-GLI3 regulation of *Pax9*, *Jag1*, and *Hes1*[17,18], however it is unknown whether any of these genes are directly responsible for SHH-GLI3 function in regulating digit number during normal autopod development or leading to the PPD pathology.

Here we define the potential role of HES1 as a novel downstream mediator of SHH/GLI3 signaling in the development of PPD. Using a series of genetic interaction and functional studies, we demonstrate that HES1 is regulated via SHH-GLI3 signaling, is sufficient to induce PPD, is required for *Gli3*-deficient PPD, and is capable of overcoming the digit number constraints of *Shh*-deficiency. Mechanistically, we show that HES1 is capable of regulating mesenchymal cell proliferation, delaying the onset of chondrogenesis, and coordinating anterior boundary formation to regulate digit number. Collectively, our data highlight a previously unknown role for HES1 as a modifier of SHH/GLI3 signaling capable of altering digit number.

Results

Hes1 over-expression is sufficient to induce preaxial polydactyly (PPD)

To determine whether *Hes1* over-expression within limb bud mesenchyme is sufficient to induce PPD, we developed conditional *Hes1* gain-of-function mutant mice that carry the *Prx1Cre* transgene and *R26-Hes1*$^{f/f}$ alleles[38–40]. *Hes1* is normally expressed within the distal posterior mesenchyme of the limb bud[33,35], however utilizing this model the expression of *Hes1* is expanded throughout the limb bud mesenchyme to recapitulate the pattern of *Hes1* expression observed within *Gli3*$^{xt/+}$ and *Gli3*$^{xt/xt}$ limb buds[33].

Skeletal analyses indicate a PPD phenotype in 91% of *Prx1Cre; R26-Hes1*$^{f/f}$ (HES1 GOF) mutant limbs as compared to wild-type (WT) littermate controls (**Fig 1A and 1B**). X-ray (**Fig 1C**) and microCT (**Fig 1D**) at 2-months of age reveal a sixth digit (red asterisk) anterior in position to digit 1. In approximately 9% of HES1 GOF mutants the sixth digit is an incomplete syndactylous digit still fused to digit one (**S1 Fig**), represented as 5.5 digits for quantitative purposes (**Fig 1B**). Most other bones in HES1 GOF mice display shortening and altered morphology[41], including fusions of several carpal/tarsal bones (**Figs 1C, 1D and S1**). When comparing the length and morphology of the additional anterior digit to other digits of HES1 GOF mice, we determined that at both E16.5 and 2-months of age (**Fig 1A, 1C, 1D and 1E**) the additional anterior digit more closely resembles that of digits 2–5. These data suggest that it is not simply a duplication of digit 1, but rather the addition of an anterior digit with more proximal digit features.

To determine the regional effects of *Hes1* over-expression on digit development, we generated *ShhCre; R26-Hes1*$^{f/f}$ mutant and controls. *ShhCre* activation induces *Hes1/Gfp* over-expression within posterior mesenchymal cells of the ZPA and their descendants that give rise

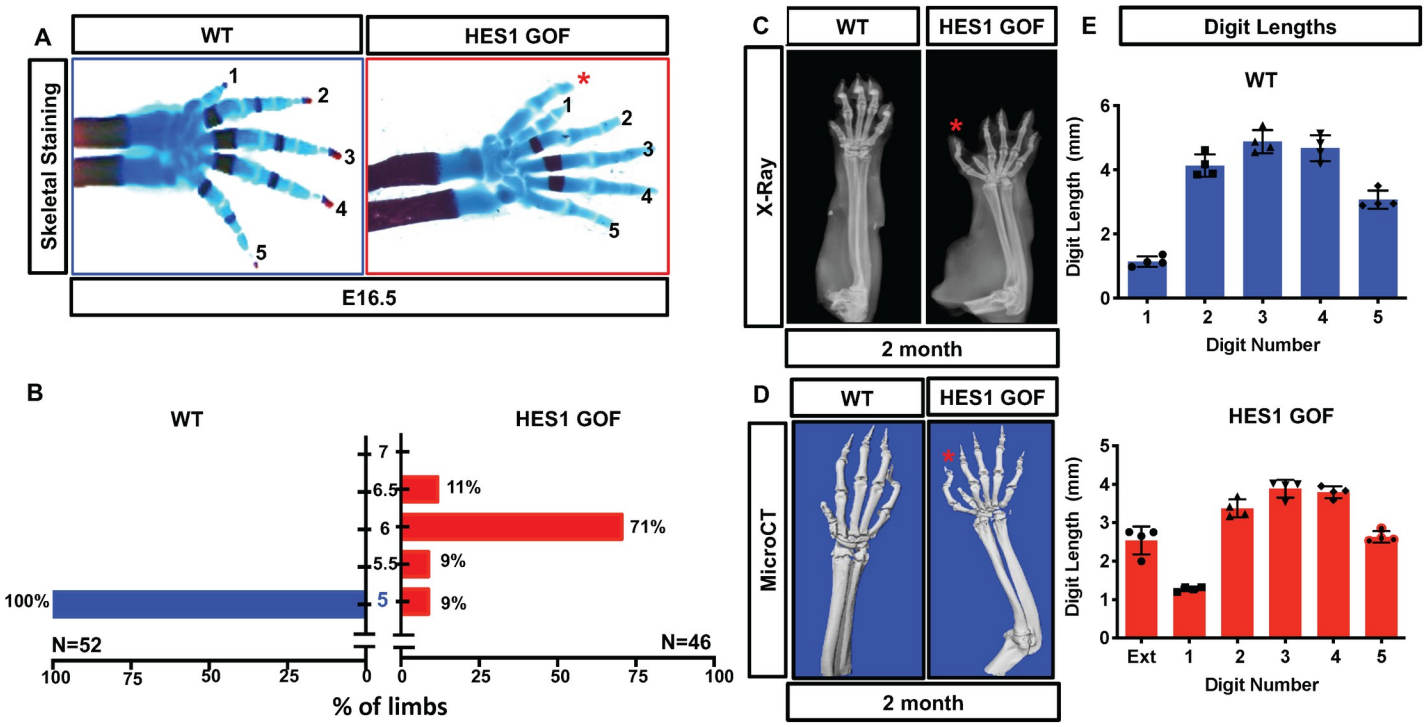

Fig 1. ***Hes1*** **over-expression within limb bud mesenchyme induces preaxial polydactyly.** **(A)** Alcian Blue/Alizarin Red staining of WT and *Prx1Cre;R26-Hes1*$^{f/f}$ (Hes1 GOF) mutant E16.5 forelimbs. Red asterisk indicates extra digit. **(B)** Quantification of digit numbers for WT (N = 52) and HES1 GOF (N = 46) forelimbs (χ^2 test) (p-value <0.0001). Y axis represents the number of digits whereas the x-axis represents the percent of the forelimbs. Intervals of 0.5 represent syndactylous digits (S1 Fig). **(C-D)** Representative X-ray and MicroCT images of 2-month old WT and HES1 GOF forelimbs. Red asterisks indicate the extra digit (N = 4) **(E)** Digit length analysis of WT and HES1 GOF at 2-months of age (N = 4).

https://doi.org/10.1371/journal.pgen.1009982.g001

to digits 4 and 5 (S2A Fig)[42]. Skeletal staining demonstrates that over-expression of *Hes1* within the posterior mesenchyme does not induce additional digit formation (S2B Fig), further suggesting that HES1 action within the anterior mesenchyme drives the PPD phenotype in HES1 GOF mice.

Hes1 over-expression within limb bud mesenchyme alters cell cycle kinetics

To determine potential mechanisms underlying HES1-induced PPD, we analyzed mesenchymal cell proliferation utilizing BrdU and phospho-histone H3 (PH3) immunohistochemistry/immunofluorescent (IHC/IF) staining. HES1 GOF limb buds display a significant increase in BrdU and PH3 positive mesenchymal cells within the apical zone, along the P-D axis, and within the anterior mesenchyme (**Figs** 2A, 2B, S3A, and S3B). Western analyses for cell cycle regulators indicate a decrease in the cell cycle inhibitor, p27, and an increase in CYCLIN D1 (CCND1) (Fig 2C) within the mesenchyme of HES1 GOF limb buds. Real-time quantitative PCR (qPCR) analyses using RNA isolated from the anterior halves of E11.5 limb buds demonstrate a mild increase in *Cdk2*, *Cdk4*, and *Cdk6* expression and confirmed the significant decrease in *Cdkn1b* expression, encoding p27 (Fig 2D). These gene expression changes were not observed in the posterior halves of HES1 GOF limb buds (S4A Fig). Since HES1 primarily acts as a transcriptional repressor[43], we searched for and identified putative HES1 binding sites (one E-box and two N-boxes) within 3kb of the *Cdkn1b* transcriptional start site (S5A Fig). Chromatin immunoprecipitation (ChIP) using HES1 antibodies on DNA isolated from E11.5 HES1 GOF and WT limb buds demonstrated that HES1 is capable of binding the

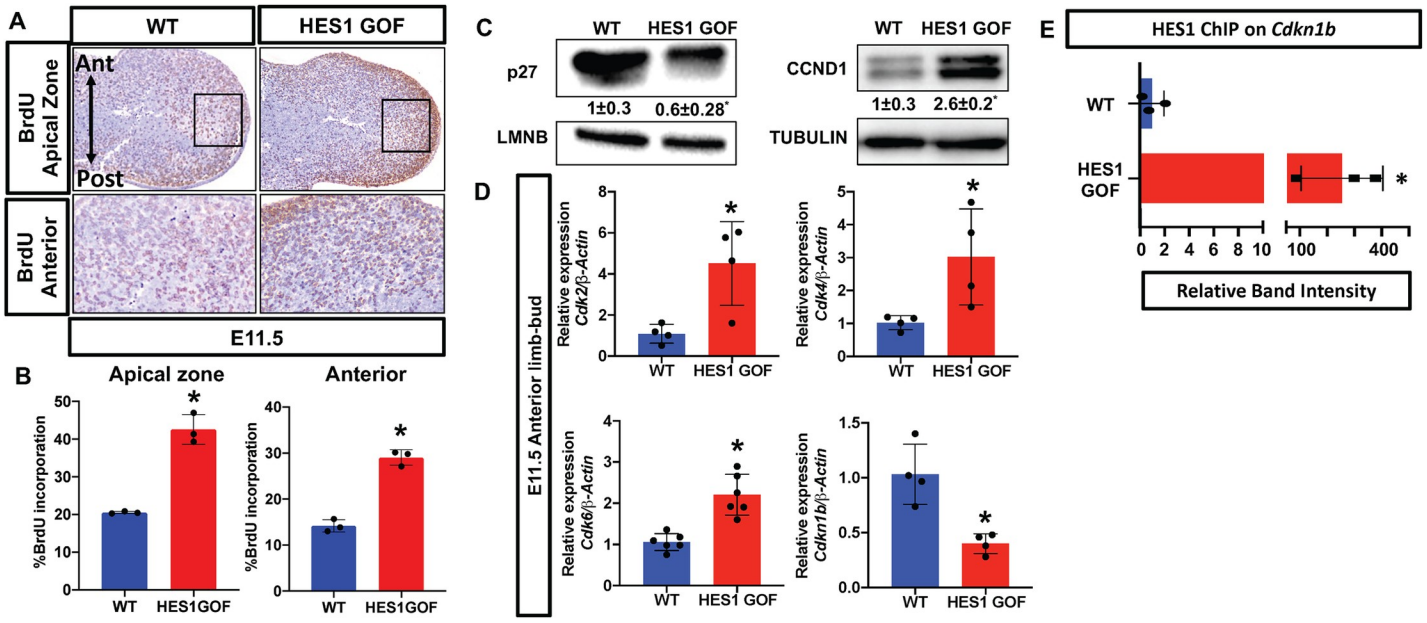

Fig 2. *Hes1* over-expression within limb bud mesenchyme promotes cell proliferation. **(A)** BrdU labeling of WT and HES1 GOF limb buds at E11.5 (N = 3) **(B)** Quantification of BrdU positive cells within the apical zone and anterior domain (N = 3). Asterisks indicate significance with a p-value < 0.05 (Student's t-test). **(C)** Western blots of p27 and CCND1 utilizing protein isolated from E11.5 WT and HES1 GOF limb buds. LMNB and TUBULIN are loading controls. Quantification represented as fold change± SD relative to WT N = 3. **(D)** qPCR for *Cdk2*, *Cdk4*, *Cdk6* and *Cdkn1b* using RNA isolated from the anterior halves of WT and HES1 GOF limb buds at E11.5 (N≥4). Each data point represents separate animals. Asterisks indicate significance with a p-value < 0.05 (Student's t-test). **(E)** Densitometry measurements of ChIP PCR amplifications from the chromatin containing an E-Box within the *Cdkn1b* promoter of WT and HES1 GOF limb buds (N = 3; p-value < 0.05; Student's t-test).

https://doi.org/10.1371/journal.pgen.1009982.g002

conserved E-box located approximately 200bp upstream of the *Cdkn1b* transcriptional start site (**Figs 2E, S5A, and S5E lanes 1–8**), but not sequences further upstream within the *Cdkn1b* promoter (**S5A Fig lanes 9–12**). This binding was substantially enriched in HES1 GOF limb buds (Fig 2E). To confirm the accuracy of our ChIP data, we also performed a positive control ChIP using HES1 antibodies on DNA isolated from E11.5 HES1 GOF and WT limb buds and demonstrated that HES1 binds to its own promoter sequence known to contain self-regulatory N-boxes (S5D Fig). These data indicate that over-expression of *Hes1* potentially enhances mesenchymal cell proliferation during limb development in part via the direct suppression of *Cdkn1b*.

Hes1 over-expression within limb bud mesenchyme delays chondrogenesis

To further investigate the effects of *Hes1* over-expression on limb development, we generated HES1 GOF and controls from E11.5 to E12.5 and performed whole-mount *in situ* hybridization (WISH), histology, IHC, and qPCR. WISH for *Sry-box 9* (*Sox9*), a transcription factor critical for forming mesenchymal condensations and chondrocyte differentiation[44], demonstrates a modest reduction in *Sox9* expression within E11.5 HES1 GOF limb buds (Fig 3A). Alcian blue staining of E12.5 HES1 GOF and WT limb bud sections demonstrates a delay in digit chondrogenesis of HES1 GOF embryos (Fig 3A). IHC analyses for COL2A1 confirm the delay in cartilage formation of HES1 GOF autopods, however proximal limb condensations eventually undergo chondrogenic differentiation leading to the formation of smaller cartilage elements (Fig 3A). qPCR performed on RNA extracted from the anterior halves at E11.5 and E12.5 demonstrate a reduction in *Sox9*, *Sry-box 5* (*Sox5*), *Sry-box 6* (*Sox6*), and *Aggrecan* (*Acan*) expression in HES1 GOF limb buds at each time point (Fig 3B). Consistent with

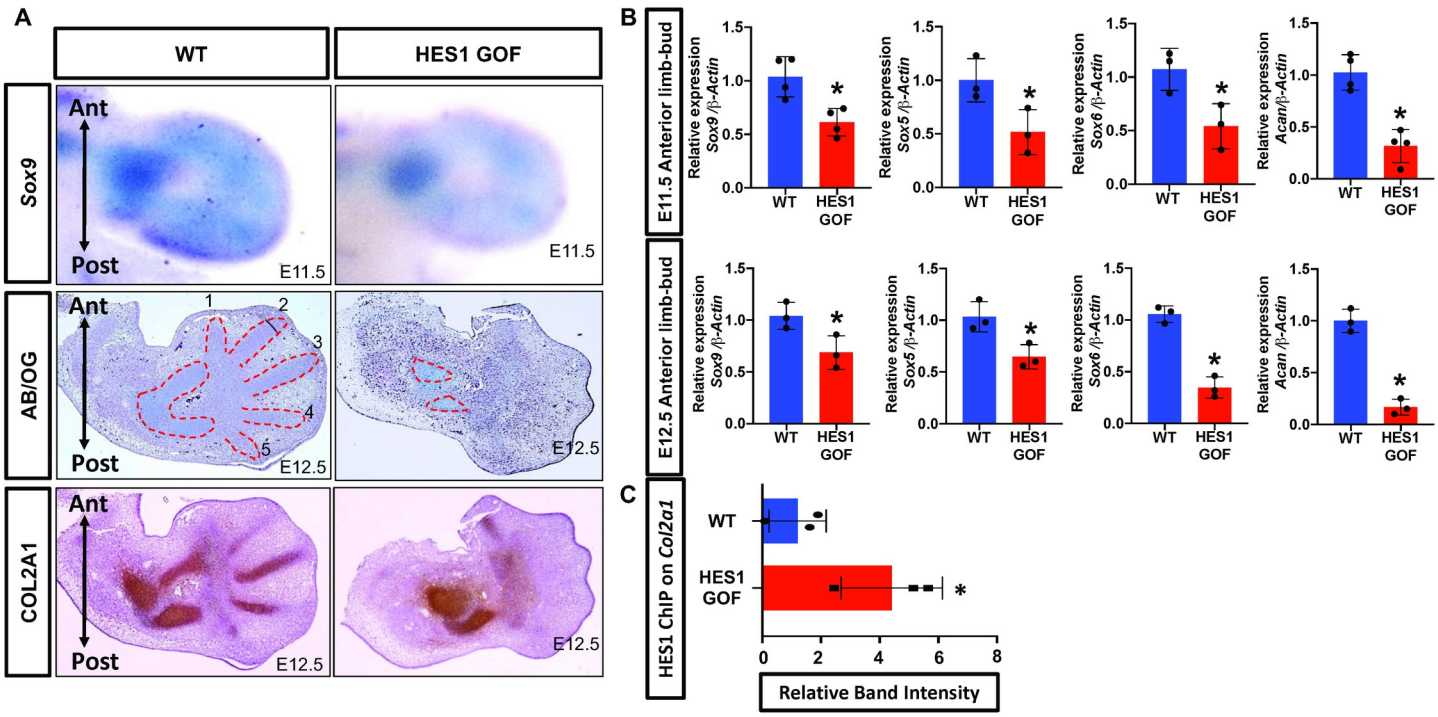

Fig 3. ***Hes1*** **over-expression within limb bud mesenchyme delays chondrogenesis. (A)** WISH for *Sox9* on WT and HES1 GOF E11.5 limb buds. ABH/OG staining of WT and HES1 GOF E12.5 limb bud sections. COL2A1 IHC staining of WT and HES1 GOF E12.5 limb bud sections. **(B)** qPCR for *Sox9*, *Sox5*, *Sox9*, *and Acan* utilizing RNA from anterior limb bud halves of E11.5 and E12.5 WT and HES1 GOF embryos ($N \geq 3$; p-value < 0.05; Student's t-test) Each data point represents separate animals **(C)** Densitometry measurements of ChIP PCR amplifications from the chromatin containing a N-Box within the *Col2a1* enhancer of WT and HES1 GOF limb buds ($N = 3$; p-value < 0.05; Student's t-test).

https://doi.org/10.1371/journal.pgen.1009982.g003

published reports[45], our sequence analyses and ChIP studies demonstrate that HES1 is capable of binding a conserved N-box within the *Col2a1* enhancer approximately 1700bp downstream of exon 1 (**Figs 3C and S5B lanes 1–8**), but not sequences further upstream within exon 1 of *Col2a1* (**S5B Fig lanes 9–12)**. This binding is enhanced in HES1 GOF limb buds (**Fig 3C**). These data indicate that over-expression of *Hes1* within limb mesenchyme delays the formation of cartilage condensations and chondrogenesis within the limb skeleton, likely via direct negative regulation of chondrogenic genes such as *Col2a1* and potentially others[41,45].

Hes1 over-expression alters several SHH/GLI-associated factors critical for digit number and patterning

To assess HES1 regulation of genes implicated in PPD, we performed WISH and qPCR for known regulators of digit number and patterning, including *Pax9*, *Alx4*, *Fgf8*, and *Bmp4*. We observed patterns of expression similar to $Gli3^{xt/+}$ and $Gli3^{xt/xt}$ mutant limb buds[32,33,46], including decreased *Pax9* expression (white arrow), restricted *Alx4* expression to the proximal mesenchyme (red arrow), expanded *Fgf8* expression within the AER (yellow arrow), and reduced mesenchymal expression of *Bmp4* (black arrows) only within the anterior limb bud (**Fig 4A**) and confirmed these results via qPCR (**Figs 4B and S4B**). These data indicate that HES1 overexpression alters the expression of several critical regulators of digit number and patterning, similar to that observed in *Gli3*-deficient polydactylies.

To determine whether *Shh* expression and SHH signaling was altered in HES1 GOF mutants, we first performed WISH and qPCR for *Shh* using whole limb buds. HES1 GOF limb

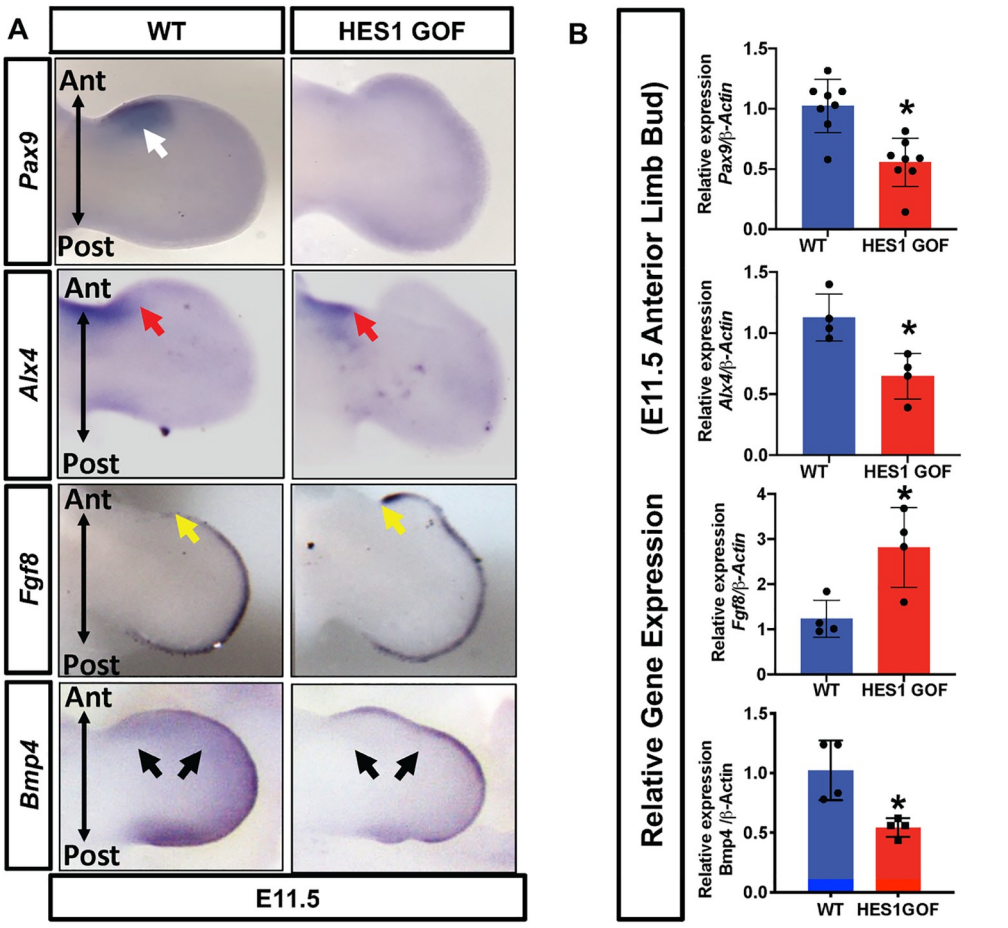

Fig 4. *Hes1* over-expression within limb bud mesenchyme alters the expression of digit patterning factors. (A) WISH for *Pax9*, *Alx4*, *Fgf8* and *Bmp4* on E11.5 WT and HES1 GOF limb buds. **(B)** qPCR performed on RNA from E11.5 WT and HES1 GOF limb buds (N≥4). Each data point represents separate animals. Asterisks indicate significance with a p-value < 0.05 (Student's t-test).

https://doi.org/10.1371/journal.pgen.1009982.g004

buds display both a mild expansion and enhancement in *Shh* expression at E11.5 (Fig 5A and 5B). To assess whether the altered *Shh* expression results in enhanced SHH signaling, we assessed SHH target gene (*Ptch1*, *Gli1*, and *Grem1*) expression and identified no changes when comparing whole limb buds, anterior halves, or posterior halves of HES1 GOF and WT limb buds via WISH or qPCR (**Figs** 5A, 5B **and** S4B). Since the processing of GLI3 from its full-length active form (GLI3A) to its repressor form (GLI3R) serves as a readout of SHH activity, we performed Westerns for GLI3 and demonstrate an unaltered ratio of GLI3R to GLI3A in HES1 GOF limb buds (Fig 5C). These data indicate that over-expression of *Hes1* within limb bud mesenchyme functions independent or downstream of SHH/GLI3/GREM1 signaling in regulating digit number.

HES1 functions independent or downstream of SHH/GLI3 and can compensate for *Shh*-deficiency

To determine whether *Hes1* over-expression can compensate for the loss of *Shh* in regulating digit number, we generated HES1 GOF mutant mice in a *Shh* conditional loss-of-function (SHH LOF) background (*Prx1Cre; R26-Hes1*$^{f/f}$*; Shh*$^{f/f}$). Skeletal analyses demonstrate that

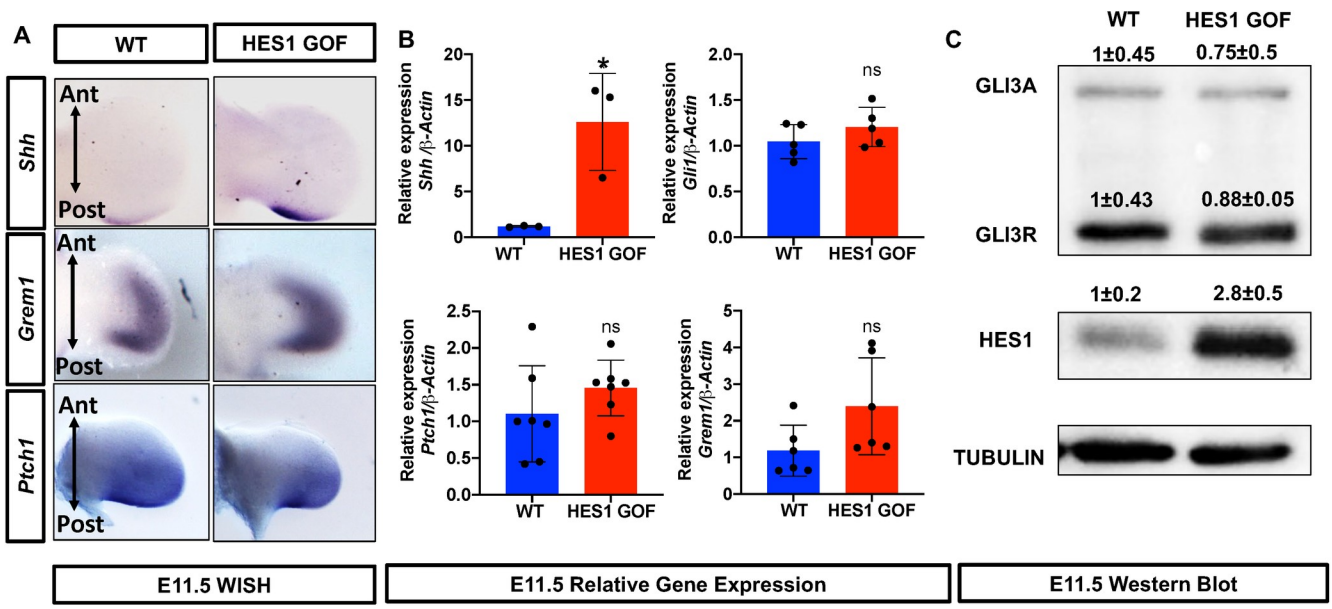

Fig 5. ***Hes1*** **over-expression within limb bud mesenchyme enhances** ***Shh*** **expression, but not SHH signaling. (A)** WISH for *Shh*, *Grem1*, *and Ptch1* on E11.5 WT and HES1 GOF limb buds. **(B)** qPCR for *Shh*, *Gli1*, *Ptch1*, *and Grem1* on RNA isolated from the anterior halves of E11.5 WT and HES1 GOF limb buds (N = 4). Asterisks indicate significance with a p-value < 0.05 (Student's t-test). **(C)** Western blots performed on protein extracted from E11.5 WT and HES1 GOF limb buds for GLI3, HES1, and TUBULIN (N = 4). Band intensities were quantified and normalized to WT for each antibody.

https://doi.org/10.1371/journal.pgen.1009982.g005

Prx1Cre; R26-Hes1$^{f/f}$*; Shh*$^{f/+}$ embryos develop a PPD phenotype similar to HES1 GOF mutants (approx. 6 digits), while *Prx1Cre; Shh*$^{f/f}$ mutants develop 1–3 digits as previously indicated (Fig 6A and 6B)[47]. Importantly, *Hes1* over-expression within the limb mesenchyme of SHH LOF mice (*Prx1Cre; R26-Hes1*$^{f/f}$*; Shh*$^{f/f}$) induces the formation of 2–5 digits in nearly 95% of double mutants (Fig 6A and 6B). Greater than 60% of double mutants develop 3 or more digits, while only 12.5% of SHH LOF mutants develop 3 digits (Fig 6A and 6B). More than 56% of SHH LOF embryos develop a single digit, while a mere 5–6% of double mutants exhibit one digit (Fig 6A and 6B). In addition to the partial rescue in digit number, we also observed a rescue of both zeugopod elements (radius and ulna) in ~10% of double mutants whereas all SHH LOF mutants develop a single zeugopod element resembling the ulna (Fig 6A). Of note, the majority SHH LOF mice die at or prior to birth, while all *Prx1Cre; R26-Hes1*$^{f/f}$*; Shh*$^{f/f}$ double mutants generated to date survive to adulthood. These results provide strong evidence that *Hes1* over-expression within *Prx1Cre*-expressing mesenchymal cells is largely capable of compensating for the loss of *Shh* in regulating digit number, patterning of the zeugopod, and survival.

To further understand the molecular mechanisms associated with these genetic changes and the corrections to SHH LOF mutant phenotypes by over-expressing *Hes1*, we performed qPCR for *Hes1* and a number of SHH targets, patterning factors, cell cycle, and cell death regulators using RNA collected from E11.5 whole limb buds of the genotypes: *Shh*$^{f/f}$ (Control), *Prx1Cre; Shh*$^{f/f}$ (SHH LOF), *R26-Hes1*$^{f/f}$*; Shh*$^{f/f}$ (Control), and *Prx1Cre; R26-Hes1*$^{f/f}$*; Shh*$^{f/f}$ (SHH LOF/HES1 GOF) (Fig 6C **and** S6A). *Hes1* expression is decreased in SHH LOF limb buds, however over-expression of *Hes1* within the limb bud mesenchyme is sufficient to drive *Hes1* expression above both SHH LOF and control levels in SHH LOF/HES1 GOF limb buds (Fig 6C). The SHH target genes, *Ptch1* and *Gli1*, are markedly reduced in SHH LOF limb buds, while over-expression of *Hes1* in the absence or presence of *Shh* is incapable of regulating their expression (**Figs** 6C**,** 5A**, and 5B**). The anti-apoptotic factor, *Bcl2*, is a direct SHH/

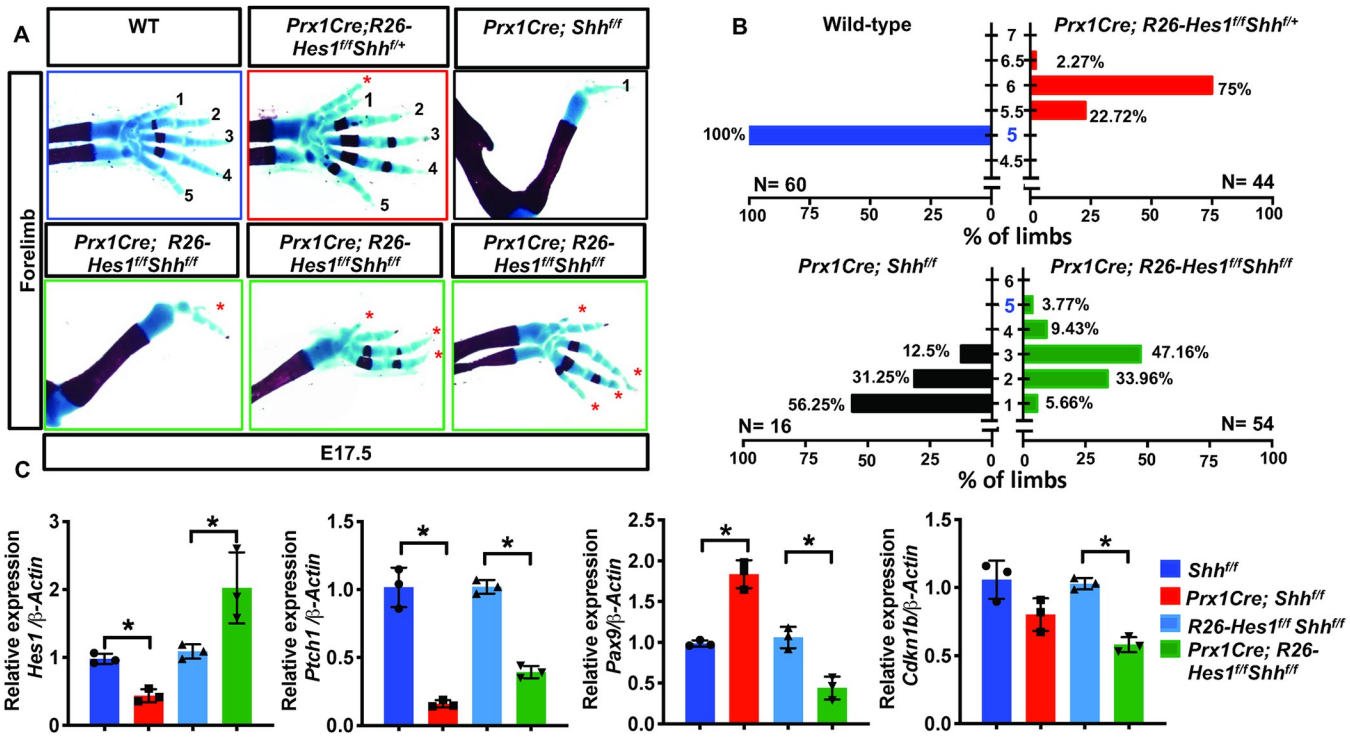

Fig 6. ***Hes1*** **over-expression within limb bud mesenchyme is sufficient to overcome the digit loss observed in SHH LOF limbs. (A)** Alcian Blue/Alizarin Red staining of WT, *Prx1Cre; R26-Hes1$^{f/f}$; Shh$^{f/+}$* (HES1 GOF), *Prx1Cre; Shh$^{f/f}$* (SHH LOF), and *Prx1Cre; R26-Hes1$^{f/f}$; Shh$^{f/f}$* (SHH LOF/HES1 GOF) double mutant forelimbs. Red asterisks indicate HES1-induced digits **(B)** Quantification of digit numbers for WT (n = 60), HES1 GOF (n = 44), SHH LOF (N = 16), and SHH LOF/HES1 GOF (n = 54) forelimbs (χ^2 test) (p-value <0.0001). Y axis represents the number of digits whereas the x-asix represents the percent of the forelimbs. Intervals of 0.5 represent syndactylous digits. **(C)** qPCR for *Hes1*, *Ptch1*, *Gli1*, *Pax9*, and *Cdkn1b* performed on RNA from *Shh$^{f/f}$* (Control), *Prx1Cre; Shh$^{f/f}$* (SHH LOF), *R26-Hes1$^{f/f}$; Shh$^{f/f}$* (Control), and *Prx1Cre; R26-Hes1$^{f/f}$; Shh$^{f/f}$* (SHH LOF/HES1 GOF) limb buds at E11.5 (N = 3). Each data point represents separate animals. Asterisks indicate significance with a p-value < 0.05 (One-way ANOVA).

https://doi.org/10.1371/journal.pgen.1009982.g006

GLI target gene[48] and an important regulator of cell death within the limb bud mesenchyme [49]. *Bcl2* expression is reduced by nearly 50% in SHH LOF limb buds, while SHH LOF/HES1 GOF displayed normal levels of *Bcl2* expression (S6A Fig). These data suggest that *Hes1* over-expression aids in reversing the cell death phenotype that occurs in SHH LOF mutant limb buds, however TUNEL staining for apoptotic cells suggests that *Hes1* overexpression alone in a WT background does not alter mesenchymal cell death (S6B Fig). Importantly, *Pax9* exhibits increased expression within SHH LOF limb buds, however over-expression of *Hes1* in the absence of *Shh* dramatically reverses this effect leading to strong suppression of *Pax9* (Fig 6C); also observed in HES1 GOF limb buds (Fig 4B). *Cdkn1b*, a negative regulator of the cell cycle and a direct target of HES1, shows no change in expression when comparing SHH LOF limb buds to controls, however forced expression of *Hes1* in the absence of *Shh* suppresses *Cdkn1b* expression (Fig 6C) similar to that observed in HES1 GOF limb buds (Fig 2D). Therefore, *Hes1* over-expression within the limb mesenchyme can reverse many phenotypic features observed in SHH LOF mutant mice, without directly affecting canonical SHH/GLI3 signaling.

HES1 and SHH/GLI3 signaling synergize to regulate digit number and gene expression

To study potential cooperative effects of HES1 and SHH/GLI3 signaling in regulating digit number, we developed HES1 GOF mutants in the *Gli3$^{xt/+}$* (GLI3 HET) background (*Prx1Cre; R26-Hes1$^{f/f}$; Gli3xt$^{/+}$)* and appropriate controls. While GLI3 HET and HES1 GOF mice exhibit

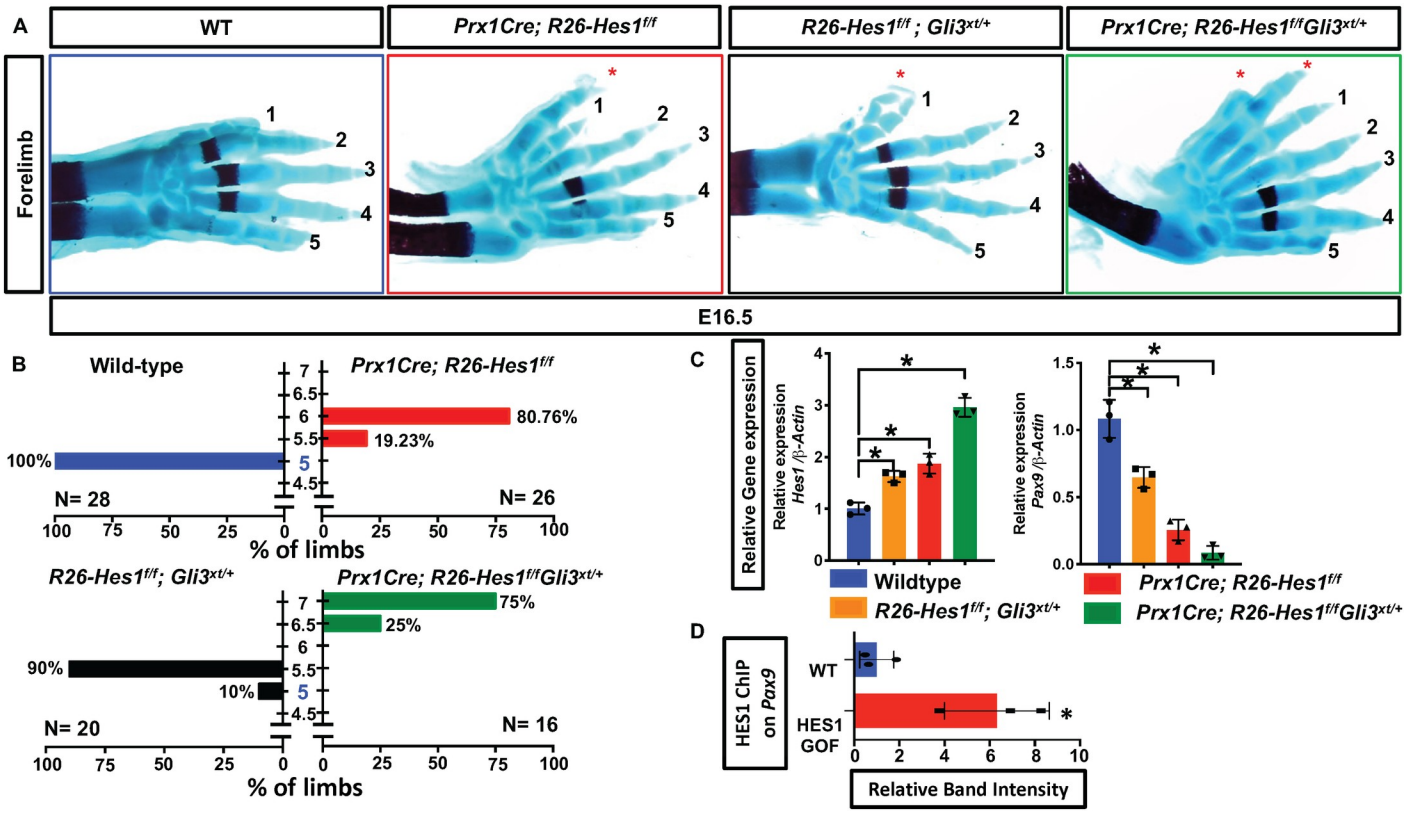

Fig 7. HES1 and SHH/GLI3 signaling cooperatively regulate digit number. (A) Alcian Blue/Alizarin Red staining of WT, *Prx1Cre; R26-Hes1*$^{f/f}$ (HES1 GOF), *R26-Hes1*$^{f/f}$*; Gli3*$^{xt/+}$ (GLI3 HET), and *Prx1Cre; R26-Hes1*$^{f/f}$*; Gli3*$^{xt/+}$ (HES1 GOF/GLI3 HET) double mutant forelimbs. Red asterisks indicate extra digits **(B)** Quantification of digit numbers for WT (N = 26), HES1 GOF (N = 28), GLI3 HET (N = 20), and HES1 GOF/GLI3 HET (N = 16) forelimbs (χ^2 test) (p-value <0.0001).). Y axis represents the number of digits whereas the x-asix represents the percent of the forelimbs. Intervals of 0.5 represent syndactylous digits. **(C)** qPCR for *Hes1* and *Pax9* on RNA from E11.5 WT, *Prx1Cre; R26-Hes1*$^{f/f}$ (HES1 GOF), *R26-Hes1*$^{f/f}$*; Gli3*$^{xt/+}$ (GLI3 HET), and *Prx1Cre; R26-Hes1*$^{f/f}$*; Gli3*$^{xt/+}$ (HES1 GOF/GLI3 HET) double mutant limb buds (N = 3). Each data point represents separate animals. Asterisks indicate significance with a p-value < 0.05 (One-way ANOVA). **(D)** Densitometry measurements of ChIP PCR amplifications from the chromatin containing an E-Box within the *Pax9* promoter of WT and HES1 GOF limb buds (N = 3; p-value < 0.05; Student's t-test).

https://doi.org/10.1371/journal.pgen.1009982.g007

5.5 digits (syndactylous 6th digit) or a complete 6 digits, the combination of these alleles induces the formation of more than 6 digits in all *Prx1Cre; R26-Hes1*$^{f/f}$*; Gli3*$^{xt/+}$ double mutants, thereby producing a more severe PPD phenotype than either single mutant alone (Fig 7A and 7B).

At the molecular level, we also observe an additive effect of these alleles on the expression of specific genes. qPCR utilizing RNA isolated from E11.5 anterior limb buds demonstrates an increase in *Hes1* expression in GLI3 HET limb buds, which was further upregulated in a progressive manner in HES1 GOF and *Prx1Cre; R26-Hes1*$^{f/f}$*; Gli3*$^{xt/+}$ double mutant limb buds (Fig 7C). Concomitantly, both qPCR and WISH analyses demonstrate a progressive downregulation of *Pax9* expression (**Figs** 7C **and** S7) while *Hes1* expression increases (Fig 7C). Due to this dynamic inverse relationship and the critical nature of *Pax9* in regulating anterior digit number[34], we performed sequence analyses of the *Pax9* promoter and ChIP for HES1. HES1 is capable of binding a specific and conserved E-box within the *Pax9* promoter located approximately 8400bp upstream of the transcriptional start site (**Figs** 7D **and** S5C **lanes 1–8**), however, was incapable of binding other upstream regions of the *Pax9* promoter (S5C Fig **lanes 9–12**). This binding was significantly enhanced in HES1 GOF limb buds (Fig 7D). Similarly, we analyzed *Alx4* promoter/enhancer sequences and could not identify obvious conserved E-

box/N-box binding sites. These data indicate that SHH/GLI3 and HES1 signals cooperate in regulating digit number and may do so in part via the direct HES1-mediated regulation of *Pax9* within the limb bud mesenchyme.

HES1 functions downstream of SHH/GLI3 signaling and is required for *Gli3*-haploinsufficient PPD

To determine whether HES1 functions downstream of SHH/GLI3 signaling and is required for *Gli3*-haploinsufficient PPD, we generated conditional homozygous deletions of *Hes1* floxed alleles within the limb bud mesenchyme of $Gli3^{xt/+}$ mutant mice (*Prx1Cre;* $Hes1^{f/f}$*;* $Gli3^{xt/+}$). Skeletal analyses demonstrate that more than 80% of the $Hes1^{f/f}$*;* $Gli3^{xt/+}$ (GLI3 HET) pups develop a syndactylous polydactyly (5.5 digits) phenotype in this genetic background, while only ~47% of the *Prx1Cre;* $Hes1^{f/f}$*;* $Gli3^{xt/+}$ mutant pups develop the same phenotype (Fig 8A and 8B). These data indicate that HES1 functions downstream of GLI3 and is largely required for the polydactyly phenotype resulting from genetic ablation of a single *Gli3* allele.

To further understand the molecular mechanisms associated with the partial genetic rescue of the $Gli3^{xt/+}$ polydactylous phenotype, we performed qPCR for *Hes1* using RNA collected from E11.5 limb buds of the following genotypes: $Hes1^{f/f}$ (WT controls), *Prx1Cre;* $Hes1^{f/f}$ (HES1 LOF), $Gli3^{xt/+}$ (GLI3 HET), and *Prx1Cre;* $Hes1^{f/f}$*;* $Gli3^{xt/+}$ (HES1 LOF/GLI3 HET) (Fig 8C). *Hes1* expression decreases in both HES1 LOF and HES1 LOF/GLI3 HET limb buds, while it increases in GLI3 HET limb buds (**Figs 8C and 7C**). These data suggest that *Hes1* is a target of SHH/GLI3 signaling in the regulation of digit number. Previous studies identified GLI factors as potential direct regulators of *Hes1*[18,50]. Therefore, we performed sequence analyses of the *Hes1* promoter and ChIP utilizing anti-GLI2 and anti-GLI3 antibodies to precipitate chromatin isolated from E11.5 WT limb buds. These data demonstrate that GLI3 and

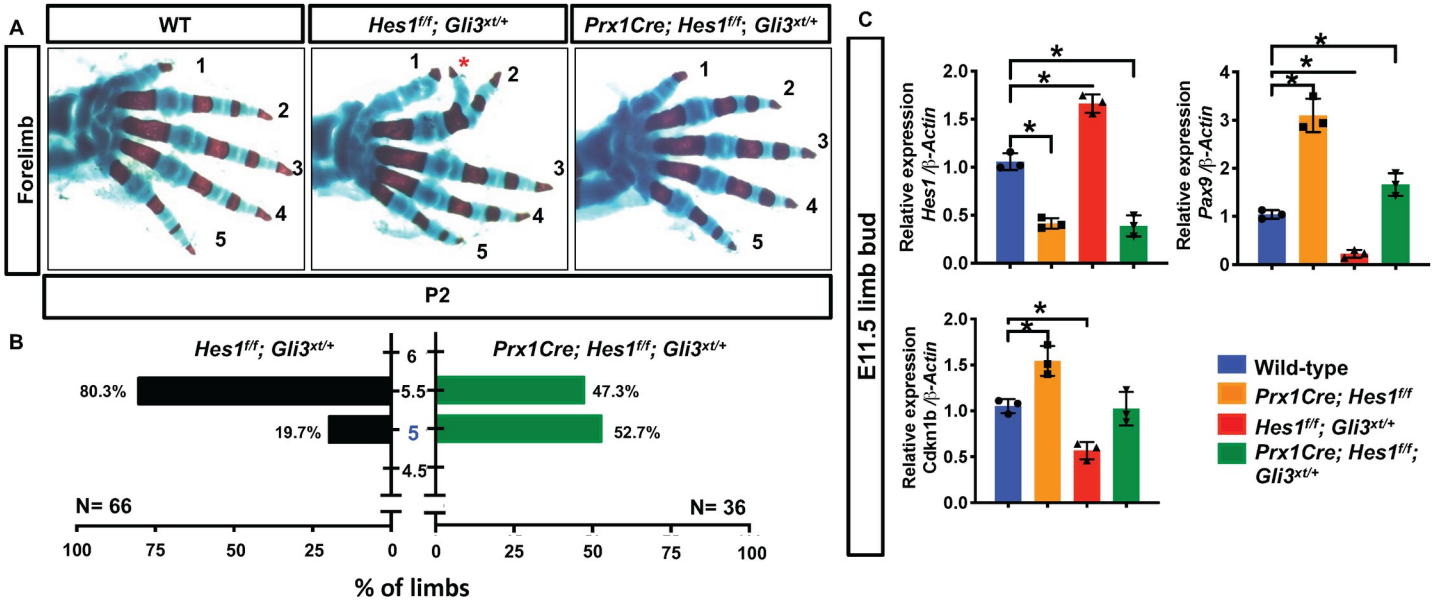

Fig 8. HES1 is a critical effector of SHH-induced PPD. (A) Alcian Blue/Alizarin Red staining of WT, $Hes1^{f/f}$; $Gli3^{xt/+}$ (GLI3 HET), and *Prx1Cre;* $Hes1^{f/f}$; $Gli3^{xt/+}$ (HES1 LOF/GLI3 HET) double mutant forelimbs. Red asterisk indicates syndactylous digit. **(B)** Quantification of digit numbers for WT, GLI3 HET (N = 66) and HES1 LOF/GLI3 HET (N = 36) double mutant forelimbs (χ^2 test) (p-value <0.0001). Y axis represents the number of digits whereas the x-axis represents the percent of the forelimbs. Intervals of 0.5 represent syndactylous digits. **(C)** qPCR for *Hes1*, *Pax9*, and *Cdkn1b* on RNA from E11.5 WT, *Prx1Cre;* $Hes1^{f/f}$ (HES1 LOF), $Hes1^{f/f}$; $Gli3^{xt/+}$ (GLI3 HET), and *Prx1Cre;* $Hes1^{f/f}$; $Gli3^{xt/+}$ (HES1 LOF/GLI3 HET) double mutant limb buds (N = 3). Each data point represents separate animals. Asterisks indicate significance with a p-value < 0.05 (One-way ANOVA).

https://doi.org/10.1371/journal.pgen.1009982.g008

GLI2 are each capable of binding two different consensus sequences within the *Hes1* promoter located approximately 146bp and 8150bp upstream of the transcriptional start site (**S9 Fig**). Collectively, these data indicate a negative regulation of *Hes1* by GLI3R within the limb bud mesenchyme during limb development.

Since we identified *Pax9* and *Cdkn1b* as potential direct HES1 gene targets during HES1-induced PPD, we assessed the expression of these genes in WT, HES1 LOF, GLI3 HET, and HES1 LOF/GLI3 HET limb buds. The expression of both *Pax9* and *Cdkn1b* are upregulated in HES1 LOF limb buds and downregulated in GLI3 HET limb buds, however HES1 LOF/GLI3 HET rescued mutant limb buds exhibit *Pax9* and *Cdkn1b* expression levels similar to or slightly higher than WT controls (**Fig 7C**). Additionally, WISH for *Pax9* and *Ptch1* demonstrate a partial rescue of the spatial expression pattern of *Pax9* in the HES1 LOF/GLI3 HET double mutants as compared to GLI3 HET, while the expression of *Ptch1* remained expanded throughout much of the mesenchyme of GLI3 HET limb buds in either the presence or absence of *Hes1* (**S8 Fig**). These data suggest that SHH/GLI regulation of digit number may be dependent on HES1 and the HES1 transcriptional regulation of *Cdkn1b* and *Pax9*, which control both proliferation of the limb mesenchyme and anterior boundaries of digit formation.

Discussion

Cooperative regulation of mesenchymal cell proliferation and chondrogenic differentiation is critical in regulating the size of the limb field and digit number. As chondrogenesis within the limb skeleton proceeds in a proximal to distal direction, the apical zone mesenchyme of the autopod is influenced by signals from the ZPA (SHH) and AER (FGFs)[1,2,9]. FGFs are required for mesenchymal cell survival and to reinforce *Shh* expression within the ZPA[7]. SHH in turn regulates mesenchymal cell proliferation by relieving GLI3 repression, resulting in the induction of *Cdk6* and *Ccnd1*, among other positive regulators of the cell cycle [17,18,32]. Additionally, SHH/GLI signaling induces *Grem1*, which functions to inhibit BMP-induced cell cycle exit and chondrogenesis to maintain apical zone mesenchymal cells in a primitive state until SHH/GLI signaling is down-regulated and BMP signals initiate the condensation of SOX9-expressing mesenchymal progenitors[32,36]. *Gli3* deficiency results in enhanced *Cdk6*, *Ccnd1*, and *Grem1* expression, which promotes expansion of the limb field via increased mesenchymal cell proliferation, delayed BMP-induced cell cycle exit, and delayed chondrogenesis. This allows for the development of additional mesenchymal condensations within the expanded autopod resulting in polydactyly[32]. Highlighting the importance of the tight control of mesenchymal proliferation and differentiation in regulating digit number, *Gli3*-deficient polydactyly is partially overcome via the conditional removal of *Cdk6* or a single copy of *Grem1*[32] or exacerbated by deletion of one or more *Bmp4* alleles[32,51]. Further demonstrating the exquisite sensitivity of this program, conditional deletion of *Bmp4*[52] alone or overexpression of *Grem1*[53] within limb bud mesenchyme delays mesenchymal cell cycle exit and the onset of chondrogenesis resulting in a polydactyly phenotype resembling that of *Gli3*-deficient mice. Here we describe a novel role for HES1 in regulating digit number in the developing autopod downstream of SHH/GLI3 signaling. Our data indicate that GLI3R directly suppresses *Hes1* expression in the anterior mesenchyme, while active SHH/GLI signaling may promote *Hes1* expression in the distal posterior mesenchyme of the developing limb bud. Mechanistically, HES1 inhibits chondrogenesis and stimulates mesenchymal cell proliferation by directly repressing chondrogenic genes (*e.g. Col2a1*) and negative regulators of mesenchymal cell proliferation (*e.g. Cdkn1b*/p27), which appears to be distinct from the positive and direct regulation of cell cycle inducers (*e.g. Cdk2*, *Cdk4*, *Cdk6*) and the activation of a potent inhibitor of BMP-induced cell cycle exit and chondrogenesis (*e.g. Grem1*) via SHH/

GLI3. Therefore, HES1 mediates unique aspects of SHH/GLI signaling to expand the limb field to the appropriate size via the regulation of both mesenchymal cell proliferation and the onset of chondrogenesis.

In addition to BMP signaling and SHH-induced regulators of the cell cycle, anterior expressed genes such as *Alx4* and *Pax9* are under the control of SHH/GLI signaling and aid in establishing anterior boundaries for autopod expansion[23,33,34,54]. ALX4 restricts the expression of *Shh* and *5'Hoxd* genes to the distal posterior mesenchyme [23,54], and inhibits cell proliferation in some contexts[55]. PAX9 is a critical regulator of A-P patterning and boundary formation in multiple tissues including the limb bud, odontogenic mesenchyme, and the palatal mesenchyme[34,56,57]. In both of the latter instances, PAX9 regulates the expression of *Bmp4* and *Msx1*, while PAX9 and MSX1 cooperatively and directly regulate the transcriptional activation of *Bmp4*[56–58]. Both *Alx4* and *Pax9* are reduced or absent in the limb mesenchyme of $Gli3^{xt/+}$ or $Gli3^{xt/xt}$ polydactylous mice and enhanced throughout the mesenchyme in $Shh^{-/-}$ limb buds[23,33,54]. Interestingly, *Bmp4* expression correlates with GLI3R levels and is subsequently reduced in the anterior mesenchyme of $Gli3^{xt/xt}$ limb buds and expressed throughout the mesenchyme of $Shh^{-/-}$ limb buds[59]. Since genetic ablation of *Pax9* and conditional inactivation of *Msx1* and *Msx2* within the limb mesenchyme results in preaxial polydactyly phenotypes resembling $Gli3^{xt/+}$ mice[34,60], it is likely that *Bmp4* expression within the anterior limb mesenchyme is transcriptionally regulated via PAX9-MSX1 in a manner similar to that observed in the odontogenic and palatal mesenchyme[57,58]. While PAX9 regulation of *Bmp4* within the anterior mesenchyme provides a likely mechanism by which PAX9 establishes an anterior boundary for digit development via regulation of cell cycle exit and chondrogenesis, the precise molecular mechanism by which SHH/GLI signaling regulates the expression of *Pax9* has remained elusive. Our data indicate an important role for HES1 downstream of SHH/GLI3 signaling to directly regulate *Pax9* expression, while no direct regulation of *Alx4* via HES1 could be identified. In *Gli3*-deficient mice, as in HES1 GOF mice, HES1 expression is observed broadly within the posterior and anterior limb bud mesenchyme resulting in the direct suppression of *Pax9* that in turn reduces the expression of *Bmp4*. Conversely, in the *Shh*-deficient limb bud, GLI3R is expressed throughout the limb mesenchyme suppressing *Hes1* expression which leads to the subsequent posterior expansion of both *Pax9* and *Bmp4;* contributing factors to *Shh*-deficient digit reductions. Collectively, all of our data are consistent with, and fit into the greater framework of, digit number regulation as demonstrated at the anatomic and molecular levels by numerous genetic models, including *Gli3*-deficiency[15,32], *Pax9*-deficiency[34], *Msx1/Msx2*-deficiency[60], *Bmp4*-deficiency[51,52], *Grem1*-over-expression[53], and *Shh*-deficiency[4,15,47], among others. Our findings further provide novel insights into SHH/GLI regulation of *Hes1*, as well as, the ability of HES1 to directly bind the promoters of *Cdkn1b* and *Pax9*, regulate their expression, and potentially their roles in coordinating digit number in the backgrounds of *Hes1* overexpression, *Gli3*-deficient polydactyly, and *Shh*-deficient digit reductions. The SHH/GLI/HES1 signaling axis identified here functions in parallel with the SHH/GLI/GREMLIN axis previously identified as a regulator of digit development[32], highlighting the complexity of integrated signals necessary to coordinate proper pentadactylous digit formation within the developing autopod and/or regulating the PPD pathology (**Fig 9**).

HES1 belongs to a class of basic Helix-Loop-Helix (bHLH) transcription factors, which bind DNA at N-box or E-box sequences to regulate or modify the expression of numerous target genes during development. The SHH/GLI signaling pathway regulates several bHLH factors important for the transcriptional control of genes coordinating digit number and patterning, including TWIST1, TWIST2, HAND1, and HAND2. Each of these bHLH factors can function as transcriptional activators and/or repressors in either homo- or heterodimeric

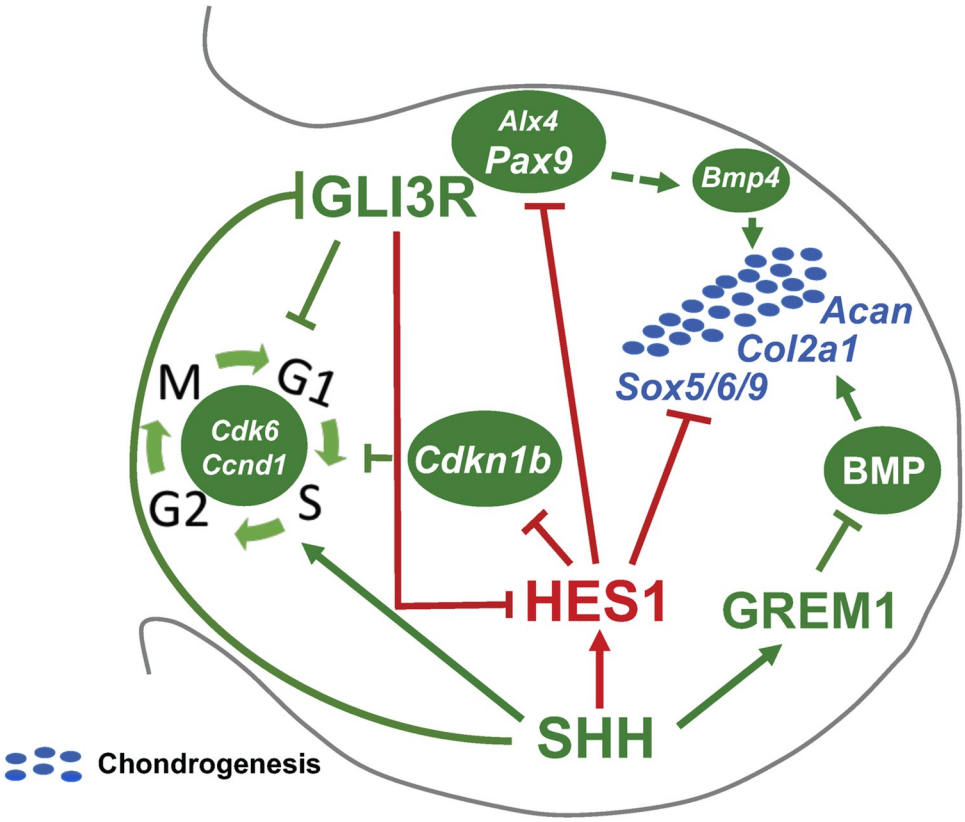

Fig 9. Proposed model for SHH/GLI3/HES1 regulation of digit number. HES1 functions downstream of SHH/GLI3 signaling to regulate digit number via: 1) a HES1-mediated transcriptional regulation of *Cdkn1b* expression to coordinate mesenchymal cell proliferation, 2) a HES1-mediated transcriptional regulation of *Pax9* to establish anterior boundaries of digit chondrogenesis, and 3) a HES1-mediated and BMP/GREM1 signaling independent transcriptional regulation that coordinates the timing of digit chondrogenesis. Red lines and arrows indicate novel findings in the SHH/GLI3/HES1-mediated regulation of digit number.

https://doi.org/10.1371/journal.pgen.1009982.g009

combinations, allowing them to regulate transcription in both active (direct binding or competitive binding of E/N-boxes) or passive (heterodimerization of activator and repressor bHLH proteins that interferes with normal DNA binding) manners. Alterations in their gene dosage via genetic deletion and/or overexpression may shift the balance and occupancy of bHLH homo- or heterodimers localized to E-boxes (or N-boxes) within a number of gene promoters/enhances important for digit number and patterning. Indeed, *Twist1*$^{+/-}$ and *Hand2*-overexpressing mice develop PPD phenotypes similar to that observed in HES1 GOF mutant mice [61]. *Twist1* is normally expressed throughout the limb bud mesenchyme, while *Hand2* and *Hes1* are natively restricted to the posterior and/or distal posterior mesenchyme [33,35,61]. Therefore, misexpression of *Hes1* within the anterior mesenchyme in HES1 GOF or *Gli3*-deficient mice[33] may cause an imbalance in bHLH homo- or heterodimer formation with TWIST1, HAND2, or other bHLH factors, while also altering their occupancy at E-box/N-box sites within the promoters/enhancers of genes regulating mesenchymal cell proliferation and differentiation or anterior boundary formation. Indeed, misexpression of *Hes1* in this way significantly alters (or induces) binding of HES1 to conserved bHLH biding sites localized to *Cdkn1b*, *Col2a1*, and *Pax9* promoters/enhancers, and likely represents a mechanism by which PPD occurs in mutants with altered *Hes1* expression. Our data shown here, as well as others assessing bHLH factors in digit number regulation, raise the intriguing possibility that

Gli3- or *Shh*-deficiencies (mutations) leading to digit abnormalities may be overcome by shifting the landscape of bHLH factor expression, interaction, and/or promoter/enhancer occupancy during critical windows of autopod development.

While we have identified HES1 as a new downstream bHLH transcriptional modifier of SHH/GLI signaling in the development of PPD, additional questions remain regarding this complex signaling control of digit development. *Hes1* is an established target gene of the NOTCH signaling pathway and the NOTCH ligand, *Jagged1*, and NOTCH target gene, *Hey1*, are also regulated via SHH/GLI signaling, raising questions as to whether the NOTCH pathway itself functions downstream or in parallel to SHH/GLI-mediated control of digit number [17,18,33,50]. Similar to our HES1 GOF mutant mice and *Gli3*-deficient mice, overexpression of the NOTCH intracellular domain (NICD) within the limb bud mesenchyme (*Prx1Cre; R26-NICD*$^{f/+}$) results in enhanced mesenchymal cell proliferation, however, completely inhibits chondrogenesis as compared to a temporary delay in chondrogenesis observed in HES1 GOF and *Gli3*-deficient limb buds[11,62]. Alternatively, conditional deletion of *Rbpjk* floxed alleles within the limb mesenchyme (*Prx1Cre; Rbpjk*$^{f/f}$) accelerates chondrogenesis and only reduces skeletal element or digit size as compared to *Shh*-deficient digit number reductions [14,62]. Interestingly, autosomal dominant forms of Adams-Oliver Syndrome (OMIM 614814, 616028, 616589) caused by germline loss-of-function mutations in *RBPjk*, *NOTCH1*, and the NOTCH ligand, *DLL4*, commonly present with abnormalities of the hands and feet including fused digits (syndactyly), severe shortening of digits (brachydactyly), and/or complete loss of digits (oligodactyly). These most severe types of digit reductions are likely not observed in our conditional NOTCH pathway loss-of-function mice (*Prx1Cre; Rbpjk*$^{f/f}$ *or Prx1Cre; Hes1*$^{f/f}$ as examples)[41,62] for a number of reasons, including NOTCH target gene redundancy (compensation via upregulation of Hes5 in the *Prx1Cre; Hes1*$^{f/f}$ mice)[41], the timing by which the *Prx1Cre* transgene induces gene deletion, or the limited expression of the transgene to the musculoskeletal limb mesenchyme. Similar differences between germline deletions and conditional deletions induced by the *Prx1Cre* transgene can be highlighted by the differential digit reductions observed in *Prx1Cre; Shh*$^{f/f}$ and *Shh*$^{-/-}$ mutant mice[14,47]. SHH/GLI signaling may indeed regulate *Hes1* in both NOTCH-dependent and -independent manners, therefore future studies will be required to tease apart whether NOTCH signaling itself is required for *Gli3*-deficient polydactyly or whether *Shh*-deficient digit restrictions can be overcome by some form of NOTCH activation.

Materials and methods

Ethics statement

All animal research performed in this study was approved by the Institution Animal Care and Use Committee (IACUC) at Duke University under protocol number A068-20-03.

Mouse strains

The *Prx1Cre* mouse line was obtained from JAX laboratory and previously described[39]. The *R26-Hes1*$^{f/f}$ [38,40] and *Hes1*$^{f/f}$ [63] mouse lines were a generous gift from Dr. Ryoichiro Kageyama (Kyoto University)[38]. The *Gli3*$^{xt/xt}$ [12] and *Shh*$^{f/f}$ [64] mutant mice were also obtained from JAX labs. All mice were housed at 23˚C on a 12 hour light /dark cycle and maintained on PicoLab Rodent Diet 290 (St. Louis, MO). Timed pregnant females were euthanized, and embryos were age-matche, stage-matched and analyzed at E10.5, E11.5, E12.5, E16.5, E18.5 and 2 months. For E11.5 analyses via WISH, qPCR, western blot and ChIP all embryos were age matched littermates and animals that displayed early chondrogenic condensations were excluded from analyses.

Whole mount skeletal staining and in situ hybridization

Whole embryo skeletal staining for digit number analysis was performed using the protocol as previously described[65]. To look at spatial-temporal expression of various genes we performed WISH on E11.5 limb buds using the previously described protocol[66].

RNA isolation and qPCR

Whole and anterior limb buds were harvested in cold 1× PBS and flash frozen using liquid nitrogen. After genotypes were obtained, mutant and wild type limb buds were pooled and homogenized in Trizol (Invitrogen) using a 25g needle. The RNA was then precipitated using 1-bromo-3-choloropropane (MRC). The aqueous layer was then separated and washed with 70% ethanol and purified using the RNeasy Plus Mini Kit (Qiagen). The RNA was transcribed into cDNA and qPCR was performed using methods described[62]. Gene expression was normalized to *Actb* followed by calculating relative expression using the $2^{-(\Delta\Delta Ct)}$ method. Mouse specific primer sequences are listed in S1 Table.

Chromatin immunoprecipitation (ChIP) assay

The ChIP assay was performed on wild type and Hes1 GOF E11.5 limb buds using the MAGnify Chromatin Immunoprecipitation system (Invitrogen) using the protocol described[41]. The HES1 antibody was a generous donation from Dr. Ryoichiro Kageyama (Kyoto University). The antibody was used at a concentration of 5 μg per reaction. Data analysis was performed using PCR primers specifically designed flanking the conserved E-box or N-box sequences within the *Cdkn1b*, *Col2a1*, *Pax9*, and *Hes1* promoter or enhancer regions, as well as, upstream negative control primers. Primers are listed in S1 Table. ChIP quantifications were performed on three gel replicates. The ImageJ software package was utilized to perform densitometry measurements of PCR bands from WT and HES1 GOF limb buds and normalized to input controls for all replicates.

Western blots

Whole and anterior limb buds at E11.5 were isolated from wild type and Hes1 GOF embryos and lysed in RIPA buffer (Invitrogen) containing protease inhibitors. The lysate was then centrifuged, the supernatant containing the protein was obtained and quantified using a BCA system. Protein (15μg) was separated using NuPAGE Novex 8% and 10% Bis-Tris pre-cast gels (Invitrogen) and was transferred to a PVDF membrane using the BIORAD system. Antibodies against HES1 (1:1000; Cell Signaling), GLI3 (1:1000; R&D systems); P27 (1:1000; BD Biosciences), CCND1 (1:1000; Cell Signaling), LMNA (1:1000; Abcam), ACTIN (1:2000; Sigma-Aldrich), and TUBULIN (1:1000; Cell Signaling) were used with the appropriate secondary antibodies.

Immunohistochemical and histological staining

Embryos were harvested in cold 1× PBS, fixed in 4% paraformaldehyde (PFA), the limbs were dissected and then hand processed. Limbs were embedded in OCT for frozen sectioning and paraffin for standard microtomy and IHC or histologic staining. Frozen sections were cut at 10μm, while paraffin sections were cut at 5μm. To analyze the general cellular morphology, standard histological staining using ABH–OG was performed. IHC was performed on paraffin sections using the VectaStain ABC kits and developed with ImmPACT DAB (Vector Labs). Primary antibodies against the following proteins were used for IHC analyses: ACAN (1:200; Chemicon), COL2A1 (1:100; Thermo Scientific), SOX9 (1:100; Santa Cruz Biotechnology),

and PH3 (1:200; Cell Signaling). Immunohistochemistry for BrdU (Invitrogen) was performed as previously described[62].

Quantification and Statistical analysis

All statistics were performed in GraphPad Prism 6 software. Statistical significance was determined by an unpaired 2-tailed Student's *t*-test or one-way ANOVA. All quantifications are represented as mean ± standard deviation. P values of less than 0.05 are considered statistically significant. All experiments were performed with N≥3 biological replicates which represent 3 or more age matched separate littermate animals. Biological replicates (N) and statistical analyses are noted within all figure legends.

Supporting information

S1 Fig. *Hes1* over-expression within limb bud mesenchyme results in defects in carpal joint formation. (A) MicroCT images of the carpal bones from WT and HES1 GOF mice at 2-month of age. hm, hamate; sc-cn, scaphoid-centrale; tq, triquetral; tm, trapezium; tz, trapezoid. Red dashed lines indicate location of carpal joints. **(B)** Alcian Blue/Alizarin Red staining of WT and *Prx1Cre;R26-Hes1*$^{f/f}$ (Hes1 GOF) mutant E16.5 forelimbs. Red asterisk indicates the syndactylous extra digit.
(TIF)

S2 Fig. *Hes1* over-expression within the posterior limb bud mesenchyme does not induce PPD. (A) GFP fluorescence from a *ShhCre; R26-Hes1*$^{f/f}$ limb bud at E11.5 and forelimb at E13.5 (N = 6). R26-Hes1 floxed allele contains and IRES-GFP labeling *ShhCre* expressing cells and their descendants. **(B)** Alcian Blue/Alizarin Red staining of WT and *ShhCre; R26-Hes1*$^{f/f}$ mutant forelimbs at E17.5 (N = 12).
(TIF)

S3 Fig. *Hes1* over-expression within limb bud mesenchyme induces phospho-histone H3. (A) Immunoflourescence for PH3 along the proximal-distal (P-D) axis and anterior mesenchyme of E11.5 HES1 GOF and WT limb buds **(B)** Quantification of PH3 positive cells along the P-D axis and anterior mesenchyme (N = 3). Asterisks indicate significance with a p-value < 0.05 (Student's t-test).
(TIF)

S4 Fig. *Hes1* over-expression within limb bud posterior mesenchyme does not affect cell cycle regulators and SHH/GLI target genes. (A) qPCR for *Hes1*, *Cdk2*, *Cdk4*, *Cdk6*, and *Cdkn1b* on RNA isolated from WT and HES1 GOF E11.5 posterior halves of limb buds (N = 3). **(B)** qPCR for *Ptch1*, *Grem1*, and *Bmp4* on RNA isolated from WT and HES1 GOF E11.5 posterior halves of limb buds (N≥3). Asterisks indicate significance with a p-value < 0.05 (Student's t-test).
(TIF)

S5 Fig. HES1 binding sites within the *Cdkn1b*, *Col2a1*, *Pax9*, *and Hes1* promoter/enhancer regions. (A) Schematic of potential HES1 binding sites within the *Cdkn1b* promoter and a schematic of conserved E-Box (HES1 binding site) within human and mouse *Cdkn1b* promoters. **(B)** Schematic of potential HES1 binding sites within the *Col2a1* enhancer region located between exons 1 and 2 and a schematic of the conserved N-Box within this region. **(C)** Schematic of potential HES1 binding sites within the *Pax9* promoter and a schematic of the conserved E-Box between mouse and human. Approximate distances in base pairs (bp) upstream of transcriptional start sites or downstream from exons are indicated for each potential HES1

binding site. **(A-D)** Representative images of ChIP PCR and controls for HES1 binding of *Cdkn1b*, *Col2a1*, *Pax9*, and *Hes1* promoters/enhancers (N = 3). N-box/E-box amplification of WT (Lane 1) and HES1 GOF (Lane 2) chromatin pulled down with anti-HES1. Amplification of WT (Lane 3) and HES1 GOF (Lane 4) chromatin pulled down with anti-HistoneH3 using RPL30 primers (positive controls). N-box/E-box amplification of WT (Lane 5) and HES1 GOF (Lane 6) chromatin pulled down with anti-IgG (negative controls). N-box/E-box amplification of WT (Lane 7) and HES1 GOF (Lane 8) input chromatin (positive controls). Non-target amplification upstream of N-box/E-box from WT (Lane 9) and HES1 GOF (Lane 10) chromatin pulled down with anti-HES1. Non-target amplification upstream of N-box/E-box from WT (Lane 11) and HES1 GOF (Lane 12) input chromatin. Non-target amplifications were not performed for the *Hes1* promoter control (D; no lanes 9–12).
(TIF)

S6 Fig. HES1 over-expression within limb bud mesenchyme restores normal levels of *Bcl2* expression in SHH LOF background and HES1 over-expression does not affect limb bud mesenchyme apoptosis. (A) qPCR for *Bcl2* on RNA isolated from WT controls ($Shh^{f/f}$) ($R26\text{-}Hes1^{f/f}$; $Shh^{f/f}$), SHH LOF (*Prx1Cre;* $Shh^{f/f}$), and HES1 GOF/SHH LOF (*Prx1Cre;* $R26\text{-}Hes1^{f/f}$; $Shh^{f/f}$) E11.5 limb buds (N = 3). Asterisks indicate significance with a p-value < 0.05 (Student's t-test). **(B)** TUNEL staining and quantification of WT and HES1 GOF limb bud sections at E11.5 (N = 3). (Student's t-test).
(TIF)

S7 Fig. HES1 over-expression further reduces *Pax9* expression in a $Gli3^{xt/+}$ background. WISH for *Pax9* on E11.5 WT, $R26\text{-}Hes1^{f/f}$; $Gli3^{xt/+}$ (GLI3 HET), *Prx1Cre;* $R26\text{-}Hes1^{f/f}$ (HES1 GOF), and *Prx1Cre;* $R26\text{-}Hes1^{f/f}$; $Gli3^{xt/+}$ (HES1 GOF/GLI3 HET) double mutant forelimbs. (N = 2).
(TIF)

S8 Fig. Removal of *Hes1* in a $Gli3^{xt/+}$ background rescues anterior *Pax9* limb bud expression without altering elevated levels of *Ptch1*. WISH for *Pax9* and *Ptch1* on E11.5 WT, $Hes1^{f/f}$; $Gli3^{xt/+}$ (GLI3 HET), and *Prx1Cre;* $Hes1^{f/f}$; $Gli3^{xt/+}$ (HES1 LOF/GLI3 HET) double mutant forelimbs (N = 3).
(TIF)

S9 Fig. GLI3 binds specific regions of the *Hes1* promoter. (A) Schematic of potential GLI binding sites within the *Hes1* promoter. **(B)** ChIP and PCR amplification of chromatin containing GLI binding sites within *Hes1* promoter (N = 3). Lane 1 = amplification of Site 1 using WT chromatin pulled down with anti-GLI3; Lane 2 = amplification of Site 2 using WT chromatin pulled down with anti-GLI3; Lane 3 = amplification of Site 1 using WT chromatin pulled down with anti-GLI2; Lane 4 = amplification of Site 2 using WT chromatin pulled down with anti-GLI2; Lane 5 = amplification of Site 1 using WT chromatin pulled down with anti-IgG (negative control); Lane 6 = amplification of Site 2 using WT chromatin pulled down with anti-IgG (negative control); Lane 7 = amplification of Site 1 using input control chromatin (positive control); Lane 8 = amplification of Site 2 using input control chromatin (positive control).
(TIF)

S1 Table. Real-time qPCR and ChIP primer sequences.
(DOCX)

S2 Table. Glossary of mutant mouse lines.
(DOCX)

S1 Data. Raw Data and Statistics.
(XLSX)

Acknowledgments

We thank Dr. Ryoichiro Kageyama (Kyoto University) for providing important *Hes1* floxed and *R26-Hes1* mouse strains, as well as, HES1 antibodies.

Author Contributions

Conceptualization: Matthew J. Hilton.

Data curation: Deepika Sharma, Anthony J. Mirando, Abigail Leinroth, Jason T. Long, Matthew J. Hilton.

Formal analysis: Deepika Sharma, Anthony J. Mirando, Abigail Leinroth, Jason T. Long, Matthew J. Hilton.

Funding acquisition: Matthew J. Hilton.

Investigation: Deepika Sharma, Anthony J. Mirando, Abigail Leinroth, Jason T. Long.

Methodology: Deepika Sharma, Anthony J. Mirando, Abigail Leinroth, Jason T. Long, Courtney M. Karner.

Project administration: Matthew J. Hilton.

Supervision: Matthew J. Hilton.

Validation: Anthony J. Mirando.

Visualization: Matthew J. Hilton.

Writing – original draft: Deepika Sharma, Matthew J. Hilton.

Writing – review & editing: Deepika Sharma, Courtney M. Karner, Matthew J. Hilton.

References

1. Chiang C, Litingtung Y, Harris MP, Simandl BK, Li Y, Beachy PA, et al. Manifestation of the limb prepattern: limb development in the absence of sonic hedgehog function. Dev Biol. 2001; 236(2):421–35. https://doi.org/10.1006/dbio.2001.0346 PMID: 11476582
2. Riddle RD, Johnson RL, Laufer E, Tabin C. Sonic hedgehog mediates the polarizing activity of the ZPA. Cell. 1993; 75(7):1401–16. https://doi.org/10.1016/0092-8674(93)90626-2 PMID: 8269518
3. Towers M, Mahood R, Yin Y, Tickle C. Integration of growth and specification in chick wing digit-patterning. Nature. 2008; 452(7189):882–6. https://doi.org/10.1038/nature06718 PMID: 18354396
4. Zhu J, Nakamura E, Nguyen MT, Bao X, Akiyama H, Mackem S. Uncoupling Sonic hedgehog control of pattern and expansion of the developing limb bud. Dev Cell. 2008; 14(4):624–32. https://doi.org/10.1016/j.devcel.2008.01.008 PMID: 18410737
5. te Welscher P, Fernandez-Teran M, Ros MA, Zeller R. Mutual genetic antagonism involving GLI3 and dHAND prepatterns the vertebrate limb bud mesenchyme prior to SHH signaling. Genes Dev. 2002; 16 (4):421–6. https://doi.org/10.1101/gad.219202 PMID: 11850405
6. Charite J, McFadden DG, Olson EN. The bHLH transcription factor dHAND controls Sonic hedgehog expression and establishment of the zone of polarizing activity during limb development. Development. 2000; 127(11):2461–70. PMID: 10804186
7. Sun X, Mariani FV, Martin GR. Functions of FGF signalling from the apical ectodermal ridge in limb development. Nature. 2002; 418(6897):501–8. https://doi.org/10.1038/nature00902 PMID: 12152071

8. Niswander L, Jeffrey S, Martin GR, Tickle C. A positive feedback loop coordinates growth and patterning in the vertebrate limb. Nature. 1994; 371(6498):609–12. https://doi.org/10.1038/371609a0 PMID: 7935794

9. Laufer E, Nelson CE, Johnson RL, Morgan BA, Tabin C. Sonic hedgehog and Fgf-4 act through a signaling cascade and feedback loop to integrate growth and patterning of the developing limb bud. Cell. 1994; 79(6):993–1003. https://doi.org/10.1016/0092-8674(94)90030-2 PMID: 8001146

10. Wang B, Fallon JF, Beachy PA. Hedgehog-regulated processing of Gli3 produces an anterior/posterior repressor gradient in the developing vertebrate limb. Cell. 2000; 100(4):423–34. https://doi.org/10.1016/s0092-8674(00)80678-9 PMID: 10693759

11. Hui CC, Joyner AL. A mouse model of greig cephalopolysyndactyly syndrome: the extra-toesJ mutation contains an intragenic deletion of the Gli3 gene. Nat Genet. 1993; 3(3):241–6. https://doi.org/10.1038/ng0393-241 PMID: 8387379

12. Maynard TM, Jain MD, Balmer CW, LaMantia AS. High-resolution mapping of the Gli3 mutation extra-toes reveals a 51.5-kb deletion. Mamm Genome. 2002; 13(1):58–61. https://doi.org/10.1007/s00335-001-2115-x PMID: 11773971

13. Chiang C, Litingtung Y, Lee E, Young KE, Corden JL, Westphal H, et al. Cyclopia and defective axial patterning in mice lacking Sonic hedgehog gene function. Nature. 1996; 383(6599):407–13. https://doi.org/10.1038/383407a0 PMID: 8837770

14. Kraus P, Fraidenraich D, Loomis CA. Some distal limb structures develop in mice lacking Sonic hedgehog signaling. Mech Dev. 2001; 100(1):45–58. https://doi.org/10.1016/s0925-4773(00)00492-5 PMID: 11118883

15. Litingtung Y, Dahn RD, Li Y, Fallon JF, Chiang C. Shh and Gli3 are dispensable for limb skeleton formation but regulate digit number and identity. Nature. 2002; 418(6901):979–83. https://doi.org/10.1038/nature01033 PMID: 12198547

16. te Welscher P, Zuniga A, Kuijper S, Drenth T, Goedemans HJ, Meijlink F, et al. Progression of vertebrate limb development through SHH-mediated counteraction of GLI3. Science. 2002; 298(5594):827–30. https://doi.org/10.1126/science.1075620 PMID: 12215652

17. Lewandowski JP, Du F, Zhang S, Powell MB, Falkenstein KN, Ji H, et al. Spatiotemporal regulation of GLI target genes in the mammalian limb bud. Dev Biol. 2015; 406(1):92–103. https://doi.org/10.1016/j.ydbio.2015.07.022 PMID: 26238476

18. Vokes SA, Ji H, Wong WH, McMahon AP. A genome-scale analysis of the cis-regulatory circuitry underlying sonic hedgehog-mediated patterning of the mammalian limb. Genes Dev. 2008; 22(19):2651–63. https://doi.org/10.1101/gad.1693008 PMID: 18832070

19. Tarchini B, Duboule D, Kmita M. Regulatory constraints in the evolution of the tetrapod limb anterior-posterior polarity. Nature. 2006; 443(7114):985–8. https://doi.org/10.1038/nature05247 PMID: 17066034

20. Knezevic V, De Santo R, Schughart K, Huffstadt U, Chiang C, Mahon KA, et al. Hoxd-12 differentially affects preaxial and postaxial chondrogenic branches in the limb and regulates Sonic hedgehog in a positive feedback loop. Development. 1997; 124(22):4523–36. PMID: 9409670

21. Zakany J, Kmita M, Duboule D. A dual role for Hox genes in limb anterior-posterior asymmetry. Science. 2004; 304(5677):1669–72. https://doi.org/10.1126/science.1096049 PMID: 15192229

22. Galli A, Robay D, Osterwalder M, Bao X, Benazet JD, Tariq M, et al. Distinct roles of Hand2 in initiating polarity and posterior Shh expression during the onset of mouse limb bud development. PLoS Genet. 2010; 6(4):e1000901. https://doi.org/10.1371/journal.pgen.1000901 PMID: 20386744

23. Kuijper S, Feitsma H, Sheth R, Korving J, Reijnen M, Meijlink F. Function and regulation of Alx4 in limb development: complex genetic interactions with Gli3 and Shh. Dev Biol. 2005; 285(2):533–44. https://doi.org/10.1016/j.ydbio.2005.06.017 PMID: 16039644

24. Hirsch N, Eshel R, Bar Yaacov R, Shahar T, Shmulevich F, Dahan I, et al. Unraveling the transcriptional regulation of TWIST1 in limb development. PLoS Genet. 2018; 14(10):e1007738. https://doi.org/10.1371/journal.pgen.1007738 PMID: 30372441

25. Zhang Z, Sui P, Dong A, Hassell J, Cserjesi P, Chen YT, et al. Preaxial polydactyly: interactions among ETV, TWIST1 and HAND2 control anterior-posterior patterning of the limb. Development. 2010; 137(20):3417–26. https://doi.org/10.1242/dev.051789 PMID: 20826535

26. Lu P, Minowada G, Martin GR. Increasing Fgf4 expression in the mouse limb bud causes polysyndactyly and rescues the skeletal defects that result from loss of Fgf8 function. Development. 2006; 133(1):33–42. https://doi.org/10.1242/dev.02172 PMID: 16308330

27. Moon AM, Capecchi MR. Fgf8 is required for outgrowth and patterning of the limbs. Nat Genet. 2000; 26(4):455–9. https://doi.org/10.1038/82601 PMID: 11101845

28. Zhang Z, Verheyden JM, Hassell JA, Sun X. FGF-regulated Etv genes are essential for repressing Shh expression in mouse limb buds. Dev Cell. 2009; 16(4):607–13. https://doi.org/10.1016/j.devcel.2009.02.008 PMID: 19386269

29. Farin HF, Ludtke TH, Schmidt MK, Placzko S, Schuster-Gossler K, Petry M, et al. Tbx2 terminates shh/fgf signaling in the developing mouse limb bud by direct repression of gremlin1. PLoS Genet. 2013; 9(4):e1003467. https://doi.org/10.1371/journal.pgen.1003467 PMID: 23633963

30. Suzuki T, Takeuchi J, Koshiba-Takeuchi K, Ogura T. Tbx Genes Specify Posterior Digit Identity through Shh and BMP Signaling. Dev Cell. 2004; 6(1):43–53. https://doi.org/10.1016/s1534-5807(03)00401-5 PMID: 14723846

31. Kozhemyakina E, Ionescu A, Lassar AB. GATA6 is a crucial regulator of Shh in the limb bud. PLoS Genet. 2014; 10(1):e1004072. https://doi.org/10.1371/journal.pgen.1004072 PMID: 24415953

32. Lopez-Rios J, Speziale D, Robay D, Scotti M, Osterwalder M, Nusspaumer G, et al. GLI3 constrains digit number by controlling both progenitor proliferation and BMP-dependent exit to chondrogenesis. Dev Cell. 2012; 22(4):837–48. https://doi.org/10.1016/j.devcel.2012.01.006 PMID: 22465667

33. McGlinn E, van Bueren KL, Fiorenza S, Mo R, Poh AM, Forrest A, et al. Pax9 and Jagged1 act downstream of Gli3 in vertebrate limb development. Mech Dev. 2005; 122(11):1218–33. https://doi.org/10.1016/j.mod.2005.06.012 PMID: 16169709

34. Peters H, Neubuser A, Kratochwil K, Balling R. Pax9-deficient mice lack pharyngeal pouch derivatives and teeth and exhibit craniofacial and limb abnormalities. Genes Dev. 1998; 12(17):2735–47. https://doi.org/10.1101/gad.12.17.2735 PMID: 9732271

35. Vasiliauskas D, Laufer E, Stern CD. A role for hairy1 in regulating chick limb bud growth. Dev Biol. 2003; 262(1):94–106. https://doi.org/10.1016/s0012-1606(03)00360-9 PMID: 14512021

36. Panman L, Galli A, Lagarde N, Michos O, Soete G, Zuniga A, et al. Differential regulation of gene expression in the digit forming area of the mouse limb bud by SHH and gremlin 1/FGF-mediated epithelial-mesenchymal signalling. Development. 2006; 133(17):3419–28. https://doi.org/10.1242/dev.02529 PMID: 16908629

37. Reinhardt R, Gullotta F, Nusspaumer G, Unal E, Ivanek R, Zuniga A, et al. Molecular signatures identify immature mesenchymal progenitors in early mouse limb buds that respond differentially to morphogen signaling. Development. 2019; 146(10). https://doi.org/10.1242/dev.173328 PMID: 31076486

38. Kobayashi T, Mizuno H, Imayoshi I, Furusawa C, Shirahige K, Kageyama R. The cyclic gene Hes1 contributes to diverse differentiation responses of embryonic stem cells. Genes Dev. 2009; 23(16):1870–5. https://doi.org/10.1101/gad.1823109 PMID: 19684110

39. Logan M, Martin JF, Nagy A, Lobe C, Olson EN, Tabin CJ. Expression of Cre Recombinase in the developing mouse limb bud driven by a Prxl enhancer. Genesis. 2002; 33(2):77–80. https://doi.org/10.1002/gene.10092 PMID: 12112875

40. Sueda R, Imayoshi I, Harima Y, Kageyama R. High Hes1 expression and resultant Ascl1 suppression regulate quiescent vs. active neural stem cells in the adult mouse brain. Genes Dev. 2019; 33(9–10):511–23. https://doi.org/10.1101/gad.323196.118 PMID: 30862661

41. Rutkowski TP, Kohn A, Sharma D, Ren Y, Mirando AJ, Hilton MJ. HES factors regulate specific aspects of chondrogenesis and chondrocyte hypertrophy during cartilage development. J Cell Sci. 2016; 129(11):2145–55. https://doi.org/10.1242/jcs.181271 PMID: 27160681

42. Harfe BD, Scherz PJ, Nissim S, Tian H, McMahon AP, Tabin CJ. Evidence for an expansion-based temporal Shh gradient in specifying vertebrate digit identities. Cell. 2004; 118(4):517–28. https://doi.org/10.1016/j.cell.2004.07.024 PMID: 15315763

43. Ohtsuka T, Ishibashi M, Gradwohl G, Nakanishi S, Guillemot F, Kageyama R. Hes1 and Hes5 as notch effectors in mammalian neuronal differentiation. EMBO J. 1999; 18(8):2196–207. https://doi.org/10.1093/emboj/18.8.2196 PMID: 10205173

44. Ng LJ, Wheatley S, Muscat GE, Conway-Campbell J, Bowles J, Wright E, et al. SOX9 binds DNA, activates transcription, and coexpresses with type II collagen during chondrogenesis in the mouse. Dev Biol. 1997; 183(1):108–21. https://doi.org/10.1006/dbio.1996.8487 PMID: 9119111

45. Grogan SP, Olee T, Hiraoka K, Lotz MK. Repression of chondrogenesis through binding of notch signaling proteins HES-1 and HEY-1 to N-box domains in the COL2A1 enhancer site. Arthritis Rheum. 2008; 58(9):2754–63. https://doi.org/10.1002/art.23730 PMID: 18759300

46. Hill P, Gotz K, Ruther U. A SHH-independent regulation of Gli3 is a significant determinant of anteroposterior patterning of the limb bud. Dev Biol. 2009; 328(2):506–16. https://doi.org/10.1016/j.ydbio.2009.02.017 PMID: 19248778

47. Zhu J, Mackem S. Analysis of mutants with altered shh activity and posterior digit loss supports a biphasic model for shh function as a morphogen and mitogen. Dev Dyn. 2011; 240(5):1303–10. https://doi.org/10.1002/dvdy.22637 PMID: 21509901

48. Bigelow RL, Chari NS, Unden AB, Spurgers KB, Lee S, Roop DR, et al. Transcriptional regulation of bcl-2 mediated by the sonic hedgehog signaling pathway through gli-1. J Biol Chem. 2004; 279 (2):1197–205. https://doi.org/10.1074/jbc.M310589200 PMID: 14555646

49. Zuzarte-Luis V, Hurle JM. Programmed cell death in the developing limb. Int J Dev Biol. 2002; 46 (7):871–6. PMID: 12455623

50. Wall DS, Mears AJ, McNeill B, Mazerolle C, Thurig S, Wang Y, et al. Progenitor cell proliferation in the retina is dependent on Notch-independent Sonic hedgehog/Hes1 activity. J Cell Biol. 2009; 184 (1):101–12. https://doi.org/10.1083/jcb.200805155 PMID: 19124651

51. Dunn NR, Winnier GE, Hargett LK, Schrick JJ, Fogo AB, Hogan BL. Haploinsufficient phenotypes in Bmp4 heterozygous null mice and modification by mutations in Gli3 and Alx4. Dev Biol. 1997; 188 (2):235–47. https://doi.org/10.1006/dbio.1997.8664 PMID: 9268572

52. Selever J, Liu W, Lu MF, Behringer RR, Martin JF. Bmp4 in limb bud mesoderm regulates digit pattern by controlling AER development. Dev Biol. 2004; 276(2):268–79. https://doi.org/10.1016/j.ydbio.2004.08.024 PMID: 15581864

53. Norrie JL, Lewandowski JP, Bouldin CM, Amarnath S, Li Q, Vokes MS, et al. Dynamics of BMP signaling in limb bud mesenchyme and polydactyly. Dev Biol. 2014; 393(2):270–81. https://doi.org/10.1016/j.ydbio.2014.07.003 PMID: 25034710

54. Panman L, Drenth T, Tewelscher P, Zuniga A, Zeller R. Genetic interaction of Gli3 and Alx4 during limb development. Int J Dev Biol. 2005; 49(4):443–8. https://doi.org/10.1387/ijdb.051984lp PMID: 15968591

55. Shi Y, Sun X, He X. Overexpression of Aristaless-Like Homeobox-4 Inhibits Proliferation, Invasion, and EMT in Hepatocellular Carcinoma Cells. Oncol Res. 2017; 25(1):11–8. https://doi.org/10.3727/096504016X14685034103833 PMID: 28081728

56. Sivakamasundari V, Kraus P, Sun W, Hu X, Lim SL, Prabhakar S, et al. A developmental transcriptomic analysis of Pax1 and Pax9 in embryonic intervertebral disc development. Biol Open. 2017; 6(2):187–99. https://doi.org/10.1242/bio.023218 PMID: 28011632

57. Zhou J, Gao Y, Lan Y, Jia S, Jiang R. Pax9 regulates a molecular network involving Bmp4, Fgf10, Shh signaling and the Osr2 transcription factor to control palate morphogenesis. Development. 2013; 140 (23):4709–18. https://doi.org/10.1242/dev.099028 PMID: 24173808

58. Kong H, Wang Y, Patel M, Mues G, D'Souza RN. Regulation of bmp4 expression in odontogenic mesenchyme: from simple to complex. Cells Tissues Organs. 2011; 194(2–4):156–60. https://doi.org/10.1159/000324747 PMID: 21546760

59. Bastida MF, Delgado MD, Wang B, Fallon JF, Fernandez-Teran M, Ros MA. Levels of Gli3 repressor correlate with Bmp4 expression and apoptosis during limb development. Dev Dyn. 2004; 231(1):148–60. https://doi.org/10.1002/dvdy.20121 PMID: 15305295

60. Bensoussan-Trigano V, Lallemand Y, Saint Cloment C, Robert B. Msx1 and Msx2 in limb mesenchyme modulate digit number and identity. Dev Dyn. 2011; 240(5):1190–202. https://doi.org/10.1002/dvdy.22619 PMID: 21465616

61. Firulli BA, Krawchuk D, Centonze VE, Vargesson N, Virshup DM, Conway SJ, et al. Altered Twist1 and Hand2 dimerization is associated with Saethre-Chotzen syndrome and limb abnormalities. Nat Genet. 2005; 37(4):373–81. https://doi.org/10.1038/ng1525 PMID: 15735646

62. Dong Y, Jesse AM, Kohn A, Gunnell LM, Honjo T, Zuscik MJ, et al. RBPjkappa-dependent Notch signaling regulates mesenchymal progenitor cell proliferation and differentiation during skeletal development. Development. 2010; 137(9):1461–71. https://doi.org/10.1242/dev.042911 PMID: 20335360

63. Imayoshi I, Shimogori T, Ohtsuka T, Kageyama R. Hes genes and neurogenin regulate non-neural versus neural fate specification in the dorsal telencephalic midline. Development. 2008; 135(15):2531–41. https://doi.org/10.1242/dev.021535 PMID: 18579678

64. Lewis PM, Dunn MP, McMahon JA, Logan M, Martin JF, St-Jacques B, et al. Cholesterol modification of sonic hedgehog is required for long-range signaling activity and effective modulation of signaling by Ptc1. Cell. 2001; 105(5):599–612. https://doi.org/10.1016/s0092-8674(01)00369-5 PMID: 11389830

65. Rigueur D, Lyons KM. Whole-mount skeletal staining. Methods Mol Biol. 2014; 1130:113–21. https://doi.org/10.1007/978-1-62703-989-5_9 PMID: 24482169

66. Rutkowski T, Sharma D, Hilton MJ. Whole-mount in situ hybridization on murine skeletogenic tissues. Methods Mol Biol. 2014; 1130:193–201. https://doi.org/10.1007/978-1-62703-989-5_14 PMID: 24482174